HEAT CAPACITY OF IRON AS A FUNCTION OF PRESSURE AND TEMPERATURE

Albert Fan Yee
(Ph. D. thesis)

November 1971

AEC Contract No. W-7405-eng-48

DISCLAIMER

Table of Contents

HEAT CAPACITY OF IRON AS A FUNCTION OF PRESSURE AND TEMPERATURE

Albert Fan Yee

Inorganic Materials Research Division, Lawrence Berkeley Laboratory
and Department of Chemistry; University of California,
Berkeley, California

ABSTRACT

A technique for the measurement of heat capacity of metals under high pressure is described. Constant current μsec pulses are used to heat the sample and the temperature rise is calculated from the change in resistance. A newly developed constant current pulse generator is described. C_p of iron was measured from 110 to 260°K and from 25 to 75 kbar. A slight decrease in C_p with pressure was noted. The increase in Debye temperature was calculated to be 4.5°K. A P-V isotherm was used to calculate the Gruneisen equation of state,

$$P = \frac{-dE_o}{dV} + \frac{0.45}{V}(E - E_o)$$

Two gamma angular correlation distribution curves from positron annihilation in ytterbium metal were taken at nine different pressures that ranged from 1 atm. to 80 kbar. There was special interest in the region of the f.c.c. to b.c.c. phase transition at 40 kbar. The observed increase in the widths of the measured curves with pressure could be entirely accounted for by the decrease in the volume of the metal with pressure. This indicates that the high pressure b.c.c. phase of Yb has only two conduction electrons per atom.

PART 1. HEAT CAPACITY OF IRON AS A FUNCTION OF PRESSURE AND TEMPERATURE

I. INTRODUCTION

The equation of state of a substance is an expression which defines all the thermodynamic variables of a substance in terms of two or more independent thermodynamic variables; two in the present study. The experimentally measurable independent variables are macroscopic manifestations of the motions of and interactions among the atoms constituting the substance. Needless to say any theory that describes the behavior of atoms in a substance must produce an equation of state that agrees with experiment. On the other hand, generalizations on classes of substances using empirical or semi-empirical equations of state enable engineers, with the aid of a few parameters, to accurately predict the behavior of any substance in a class under various conditions. Thus the importance of equations of state is clear.

The existence of regular crystalline structure in most solids renders their theoretical equations of state particularly interesting. Unfortunately, the experimental measurements are difficult. The most direct technique is the measurement of volume change as a function of temperature and pressure. This can be accomplished by piston displacement or X-ray techniques. More indirectly, the measurements of heat capacity and elastic constants can also yield equations of state.

The piston displacement technique[1-3] is limited by the precision with which one can determine volume changes, especially in a piston-cylinder device where the deformation and friction increase with

increasing pressure. The pressure attainable is limited to 20 kbar in an unsupported system, and 50 kbar when supported. Useful data can be obtained only on very compressible substances such as the alkali metals and solidified gases. Bridgman produced vast amounts of P-V data near room temperature on various substances using this technique. The X-ray technique suffers from difficulties in the precision as well as the analysis of data.[4,5] When combined with a P-V isotherm, the equation of state as well as all other thermodynamic functions can be calculated from the heat capacity measured as a function of temperature and pressure. Because of the large thermal mass of the high pressure bomb, only those substances with heat capacities substantially larger than that of the bomb can utilize direct calorimetry. Consequently, only substances such as solidified gases which have relatively higher molar heat capacities at low temperatures, and substances that undergo phase transitions which result in large changes in heat capacities have been measured: calorimetric determinations of the heat capacities of solid He,[6,7] solid H_2,[8] uranium,[9] and cerium[10] have been carried out to a maximum of 20 kbar. Ultrasonic methods, in principle, can yield the most precise results. Unfortunately, severe problems in experimental techniques are encountered at pressures above 10 kbar.[11]

Out side the domain of static pressures, shock techniques have produced large amounts of ultra high pressure, high temperature PVT data.[12,13] Data below 100 kbar using this technique rapidly become unreliable. It is also difficult to extraploate these high temperature and high pressure data to more moderate conditions. However progress is being made in correlating static pressure and shock results.[14]

Sometimes valuable data can be obtained by using theoretical approximations and indirect measurements. One such case is the work by Raimondi and Jura.[15] They used the Bloch-Gruneisen equation to calculate the Debye temperature and hence the Mie-Gruneisen equation of state of aluminum from its resistance measurements as a function of temperature and pressure. This method applies only to simple, "good" metals, but has the advantage of being relatively simple and precise.

It is obvious that none of the methods discussed thus far fulfill all the requirements of high precision, wide temperature and pressure range and flexibility with respect to the type of substance that can be used. Each of the methods is useful within its limits. All of them have been and are employed in order to produce data in the widest range possible. Difficulties arise when one attempts to correlate data from these various sources. First of all, a pressure gap exists between 20 kbar and 100 kbar, and similarly a temperature gap between 40°K and several hundred or even thousand degrees Centigrade. Secondly, only rare gases, alkali metals and a few special interest metals such as those that exhibit phase transitions at low temperatures have been investigated at the low ends of pressure and temperature.

The present work is a continuation of the effort begun by Stark[16] to measure the heat capacity of metals under pressure. Stark used a pulse heating method similar to that of Wallace et al.[17] Some of his electronic instruments introduced serious errors in his results which are difficult to assess. His most serious error will be discussed later. He measured the heat capacities of gadolinium, iron

and bismuth as functions of pressure. For gadolinium he was able to measure the change in Curie temperature with pressure. For iron the heat capacity did not change within his experimental error. For bismuth he determined the thermodynamic value for the pressure of the III-V phase transition.

In this work a successful effort was made to improve the pulse heating technique. A constant current pulse generator was developed. The measurement techniques for the various quantities were carefully examined and improved when possible. Heat capacity of iron was measured from 110 to 260°K and from 25 to 75 kbar. The error for each single measurement is estimated to be 3 to 4% but the results show surprising consistency. The Gruneisen equation of state was calculated.

Iron was chosen for this work partly because it was the metal on which the most extensive research was performed by Stark, and partly because it has the optimum combination of high resistivity and high Debye temperature, both of which are desirable for this work.

II. THEORY

A. Equation of State

It has been pointed out in the Introduction that the equation of state of a solid can be calculated from a P-V isotherm and from the heat capacity measured as a function of temperature and pressure. We will now see how this may be accomplished and whether it is applicable to the present experiment.

If we integrate both sides of the thermodynamic identity

$$\left(\frac{\partial C_p}{\partial P}\right)_T = -T\left(\frac{\partial^2 V}{\partial T^2}\right)_P \tag{1}$$

we get

$$\int_{T_1}^{T_2} \left(\frac{\partial C_p}{\partial P}\right)_T d\ell nT = -\left(\frac{\partial V}{\partial T}\right)_P\Bigg|_{T_2} + \left(\frac{\partial V}{\partial T}\right)_P\Bigg|_{T_1} \tag{2}$$

But

$$\left(\frac{\partial V}{\partial T}\right)_P = \left(\frac{\partial S}{\partial P}\right)_T \tag{3}$$

At 0°K, for a perfect crystal, S=0, so

$$\left(\frac{\partial S}{\partial P}\right)_{T=0} = 0 = \left(\frac{\partial V}{\partial T}\right)_P\Bigg|_{T_1=0} \tag{4}$$

If we make T_1 in Equation (2) equal to 0°K, then Equation (2) reduces to

$$\int_{o}^{T_2} \left(\frac{\partial C_p}{\partial P}\right)_T d\ell n\, T = - \left(\frac{\partial V}{\partial T}\right)_P \Bigg|_{T_2} \qquad (5)$$

Let us consider Figs. 1 and 2. Figure 1 is the room temperature isotherm for the reduced volume vs. pressure for iron compiled by Stark[16] from several sources. Figure 2 is a hypothetical plot of $\left(\frac{\partial C_p}{\partial P}\right)_T$ vs. T for several different pressures. Equation (5) enables us to calculate $\left(\frac{\partial V}{\partial T}\right)_P$ at any temperature T_2 and pressure, provided we have available to us data such as those illustrated in Fig. 2. Then, given an isotherm such as the one in Fig. 1, we will be able to generate the entire P-V-T surface.

In order to obtain results such as those in Fig. 2, we must have a large amount of C_p data which are sufficiently accurate and situated at small temperature and pressure intervals. At the present stage of experimental development this approach does not yet appear to be feasible. Instead we will make a few assumptions and make use of the familiar Gruneisen equation of state.

The equation of state of solid may be expressed as

$$P = P(V,T) \qquad (6)$$

One could expand Equation (6) in a power series, as Slater[18] did But power series expressions tend to mask the physical meanings contained in them. From thermodynamics, one finds

$$P = - \left(\frac{\partial A}{\partial V}\right)_T \qquad (7)$$

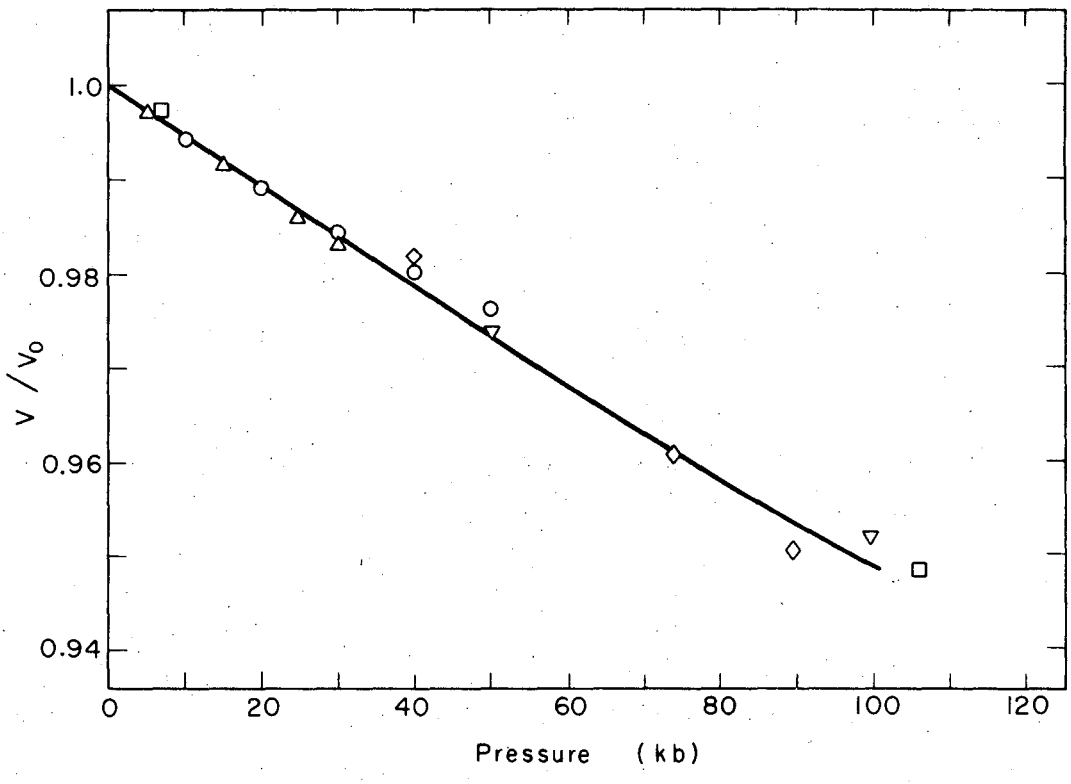

XBL673-2261

Fig. 1. Reduced Volume of Iron vs. Pressure

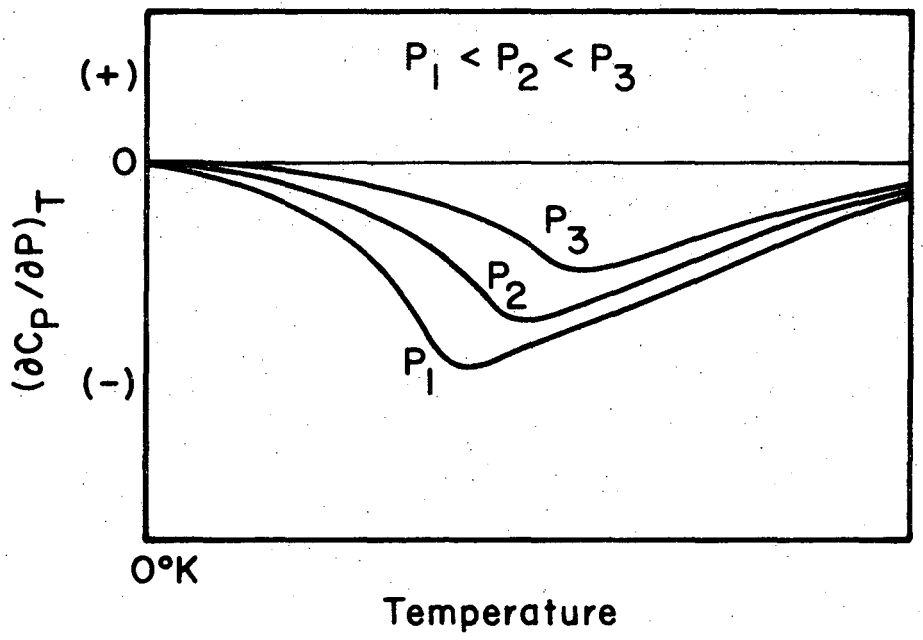

XBL 7110-7444

Fig. 2. Hypothetical $\left(\frac{\partial C_p}{\partial P}\right)_T$ isobars as function of temperature.

where A is the Helmholtz free energy. One also finds from statistical mechanics that

$$A = - kT\ell nZ \tag{8}$$

where Z is the partition function of the system under consideration. Therefore

$$P = kT\left(\frac{\partial \ell nZ}{\partial V}\right)_T \tag{9}$$

In other words, if we know the partition function Z and its variation with volume, we have the equation of state. Consider a solid consisting of atoms occuping lattice sites. Z can be found only if we know the frequency distribution function $g(\nu)$ of the lattice. Due to the large number of normal modes in a crystal, sampling techniques had to be used by Garland and Jura[19] to obtain an approximation to the spectrum of an f.c.c. lattice. This is a rather difficult and tedious process.

Even when we have the frequency distribution function $g(\nu)$ of a solid it would still be impossible to predict how $g(\nu)$ changes with volume. Grüneisen suggested that the variation of each normal mode with respect to volume obeys the following relationship:

$$\gamma_j = \frac{-d\ell n\ \theta_j}{d\ell nV} \tag{10}$$

where θ_j is the characteristic temperature for the normal mode j and $\theta_j = h\nu_j/k$, and γ_j is a constant. Barron[20] has discussed the validity

of this assumption and has shown that it is generally a good approximation at high temperatures.

Now we can write, to a good approximation,

$$A = E_o(V) + A^*(V,T) = E_o(V) + \sum_{j=1}^{N} A^*_j(V,T) \tag{11}$$

where $E_o(V)$ is the internal energy at 0°K and is therefore independent of temperature, and $A^*(V,T)$ is the thermal energy due to the lattice vibration. The contributions from the excited states have been assumed to be mutually independent.

Thus, from Equation (7)

$$P = P_o(V) + P^*(V,T) \tag{12}$$

where $P_o(V)$ is the "internal pressure" necessary to obtain a volume V at 0°K and $P^*(V,T)$ is the "thermal pressure". Equation (12) may again be rewritten as

$$P = -\frac{dE_o}{dV} + \sum_{j=1}^{N} \frac{\gamma_j E_j^*(\theta_j/T)}{V} \tag{13}$$

This is the familiar Mie-Grüneisen equation of state, which is essentially a form of a law of corresponding states.

A further simplification occurs if one uses the Debye approximation for the frequency distribution.†

---

† It is not necessary to use the Debye approximation to obtain Equation (15). It is introduced here for the convenience of subsequent discussions.

For a continuum solid, $g(\nu)$ is proportional to ν^2. To account for the discrete nature of the lattice, Debye imposed a maximum frequency ν_{max} on $g(\nu)$ such that

$$\int_0^{\nu_{max}} g(\nu)d\nu = 3N \tag{14}$$

ν_{max} has a wavelength approximately equal to the lattice constant. Given this approximation, Equation (14) reduces to

$$\gamma = \frac{-d\ell n\theta_D}{d\ell nV} \tag{15}$$

where $\theta_D = h\nu_{max}/k$ and is known as Debye temperature.

Now we may rewrite Equation (13) again:

$$P = \frac{-dE_o}{dV} + \frac{\gamma}{V}(E - E_o) \tag{16}$$

where

$$E - E_o = 9RT\left(\frac{T}{\theta_D}\right)^3 \int_0^{\theta_D/T} \frac{u^3 du}{e^u - 1} \tag{17}$$

and u is a dummy variable.

It is now obvious that if we can measure C_v as a function of P and T, then the equation of state is uniquely determined when a P-V isotherm is available.

B. Heat Capacity

The heat capacity C_v of a metal consists usually of the lattice heat capacity C_v^{ℓ} and the electronic heat capacity C_v^e. In the case of a ferromagnetic metal there is also the additional magnetic heat capacity C_v^m, which becomes very large near the Curie temperature, T_c. The effect of pressure on these heat capacities will now be discussed.

The theories of lattice heat capacity, i.e., the Einstein and Debye theories and the rigorous treatment by Born and von Karman are familiar and can be found in standard textbooks such as Kittel[21] and the review article by Blackman.[22] These theories are normally used to describe the variation of heat capacity with temperature. The pressure effect on lattice heat capacity can be derived from these same theories if one considers its effect on the energy levels: as the lattice spacing decreases the energy levels become higher, which is to say the number of available states at a given finite temperature decreases. Thus statistical mechanics predicts decreasing heat capacity with increasing pressure. From Equation (14) it can be easily seen that if the density of states $g(\nu)d\nu$ decreases ν_{max} must increase because the integral is a constant. It follows immediately that θ_D must also increase since $\theta_D = h\nu_{max}/k$. This observation is naturally consistent with the prediction that C_v must decrease.

The electronic heat capacity[21] of a metal depends on the temperature T and the density of states at the Fermi surface $D(\epsilon_F)$:

$$C_V^e = \frac{1}{3}\pi^2 D(\epsilon_F) k^2 T \qquad (18)$$

where k is Boltzmann's constant. For a simple metal Equation (18) reduces to

$$C_v^e = \frac{1}{2}\pi^2 Nk \frac{T}{T_F} \tag{19}$$

where $T_F = \frac{\epsilon_F}{k}$ and is known as Fermi temperature. For most metals it is several tens of thousand degree K, so at room temperature C_v^e is very small compared with C_v $D(\epsilon_F)$ is usually much larger for transition metals than for transition metals than for simple metals because of the narrow d band,† hence transition metals usually have a larger contribution to their heat capacities from electrons than do the simple metals. It is difficult to estimate quantitatively how much C_v^e will change for a given volume change for a transition metal, although the same argument based on the separation between energy levels applies and would predict decreasing heat capacity with increasing pressure provided the electronic structure does not change. For a simple metal, where the Fermi energy is inversely proportional to the cube root of the volume,[21] we can easily calculate from Equation (19) what the change should be. In general, we will find that this change is small compared to the change in C_v^ℓ at or below room temperature.

The effect of pressure on C_v^m is even more difficult to predict. The magnetic heat capacity[23] arises from the coupling of the spins of the electrons in the d or f band of a transition metal. It is

---

† The discussion here applies also to transition metals with unfilled f bands.

usually obtained by subtracting C_v^{ℓ}, C_v^e and the dilation term $C_p - C_v$ from C_p. One result for iron is shown in Fig. 3.[24] The Curie temperature is 1043°K. At room temperature and one atmosphere, C_v^m is about 2% of the total C_p. Throughout the temperature range of these experiments, C_v^m is equal to or less than 2%. It should be borne in mind that such a dissection depends on the correctness of the theories on which it is based.[25] C_v^m may be written

$$C_v^m = Bf\left(\frac{T}{T_c}\right)^r \tag{20}$$

where B is a constant and the value of r depends on the theory and the temperature range.[23,25,26] Thus the question of the pressure effect on C_v^m reduces to one of the pressure effect on T_c. For iron Patrick[27] measured dT_c/dP to 9 kbar and found it essentially zero. More recently Léger et al.[28] repeated the experiment to 17 kbar and found dT_c/dP zero also. According to the existing theories, then, C_v^m for iron does not change with pressure.

Finally, the effect of pressure on the dilation heat capacity must be considered. From thermodynamics, we find

$$C_p - C_v = \frac{V_o T \alpha^2}{\chi} \tag{21}$$

where α is the coefficient of thermal expansion and χ is the compressibility. For most metals both α and χ are quite small and their pressure variation can be considered negligible. Indeed, one of the results of the present investigation is that the pressure dependence of α is very small.

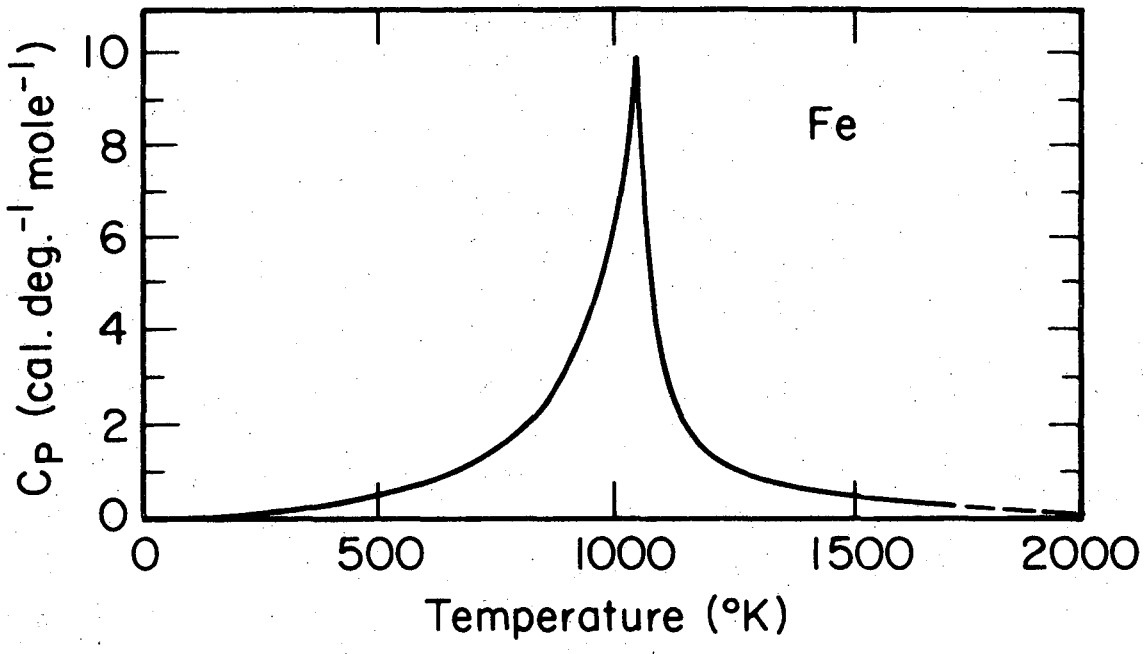

XBL 7110-7445

Fig. 3. Magnetic Heat Capacity of Iron

C. Heat Capacity Measurement

It has been pointed out in the Introduction that the conventional calorimetric technique is not suitable for measurement of heat capacity under high pressure because of the extremely large thermal mass of the high pressure apparatus. The pulse heating technique employed in this work sends a pulse of energy of a predetermined magnitude into the sample and the temperature rise of the sample is measured; no knowledge of the heat capacity of the surroundings is necessary.

Heat capacity at constant pressure is

$$C_p = \left(\frac{\partial H}{\partial T}\right)_P \tag{22}$$

where H is the enthalpy. Experimentally we apply a small amount of heat to the sample and observe its temperature rise:

$$C_p = \frac{\Delta H}{\Delta T} \tag{23}$$

It is an experimental fact that Joule heating occurs if we pass an electrical current I through a resistor of resistance R; the power developed is

$$P = \frac{dH}{dt} = I^2 R \tag{24}$$

If we want the power input to be constant, and if we assume that the resistance change is negligible, then the current must be constant. It was found, indeed, that the assumption of constant power input is valid within experimental error. As soon as the current starts

flowing, the temperature of the resistor begins to rise at a rate according to the time derivative of Equation (23):

$$\frac{dT}{dt} = \frac{1}{C_p} \frac{dH}{dt} = \frac{1}{C_p} I^2R \tag{25}$$

assuming C_p does not change during this time interval. Suppose we know the temperature dependence of the resistor, i.e.,

$$R = R(T) \tag{26}$$

and

$$R' = \frac{dR(T)}{dT} \tag{27}$$

then by measuring the rate of change of resistance we can calculate the rate of change of the temperature:

$$\frac{dT}{dt} = \frac{1}{R'} \frac{dR}{dt} \tag{28}$$

Equating Equations (25) and (28) and rearranging, we get

$$C_p = \frac{I^2RR'}{\frac{dR}{dt}} \tag{29}$$

The best way of measuring the resistance change is by measuring the voltage drop across the sample and using Ohm's law E = IR. We finally get

$$C_p = \frac{I^3 R R'}{\frac{dE}{dt}} \tag{30}$$

To summarize, if we know the resistance of our metal sample and its dependence on temperature, and if we pass a constant current pulse through the sample, then by measuring the rate of change of the voltage drop across the sample we can calculate the heat capacity according to Equation (30).

In practice, the situation is of course not so simple. Assuming that we can produce the current pulse and measure each of the quantitites without difficulty, we are still faced with the problem of having neglected the heat leak from the sample to its surroundings. Carslaw and Jaeger[29] analyzed the case of heat conduction from a circular rod to its surrounding, which is analogous to our case of heat leak from a wire-shaped sample to the pressure transmitting medium, and concluded that the heat flux across such a boundary is proportional to the temperature difference across the boundary.

When such a heat leak exists, the net power input to the sample is

$$\frac{dH}{dt} = I^2 R - K(T - T_a) \tag{31}$$

where K is a coefficient of power conduction across this boundary and T_a is the temperature of the medium. Replacing Equation (31) for Equation (24) in Equation (25), we have

$$\frac{dT}{dt} = \frac{1}{C_p} \frac{dH}{dt} = \frac{1}{C_p} [I^2 R - K(T - T_a)] \tag{32}$$

Again equating Equation (32) to Equation (28), applying Ohm's law, and rearranging, we have

$$\frac{dE}{dt} = \frac{I^3RR'}{C_p} - \frac{IR'}{C_p} K(T - T_a) \qquad (33)$$

It is obvious that if we are able to measure the initial slope before the temperature gradient becomes significant, the heat leak error would be minimized. Whether the slope measured has a negligible amount of heat leak error becomes evident if we pulse the sample with several different currents and then plot $\frac{1}{I} \frac{dE}{dt}$ vs. I^2. If the plot is linear and has zero intercept, the heat leak effect can be ignored. Otherwise we expect to see a significant negative intercept, a result often obtained in Stark's work.[16]

III. EXPERIMENTAL

A. High Pressure Assembly and Sample

The ideal high pressure apparatus would be a piston-cylinder assembly with a perfectly non-viscous and incompressible fluid as the pressure transmitting medium. In such a system the pressure would be completely hydrostatic and furthermore it can be simply calculated by knowing the force applied on the piston and the piston end surface area. Unfortunately, as the pressure is increased both the piston and the cylinder become mechanically deformed, load and force no longer enjoy a simple relationship because of the increased friction, and eventually the entire assembly becomes so deformed that it is rendered useless. To further complicate the problem, very few fluids are available which will not freeze into a solid beyond a few tens of kbars even at room temperature. Simple piston-cylinder devices are able to generate pressures up to approximately 50 kbars.[30] Multiple stage piston-cylinder devices are available which are capable of generating up to 100 kbars;[31] but these are expensive and complicated systems using solids for pressure transmitting media. When higher pressures are desired, or when the piston-cylinder geometry is not suitable for the experiment to be performed, other less ideal systems have to be employed.

In these experiments high pressure was generated by the Bridgman opposed-anvils system (Fig. 4). The system consists of a pair of cylindrically shaped cemented tungsten carbide pieces each surrounded by a circular block of high strength heat-treated steel, forming the so-called Bridgman anvils. The tungsten carbide cylinders have an approximately 1° taper, a flat surface at one end and are machined

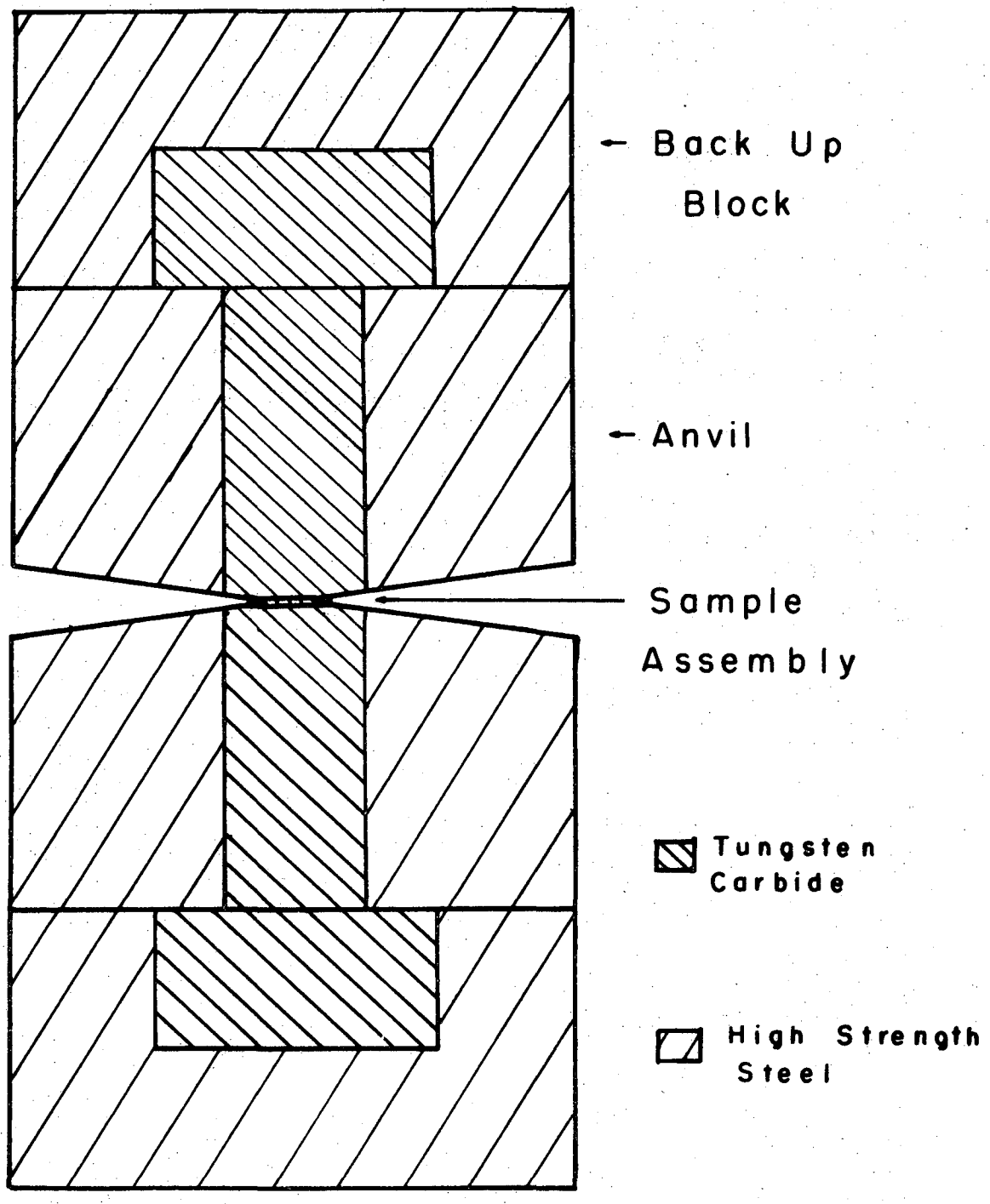

XBL 707-1506

Fig. 4. Bridgman Opposed-Anvils

into a truncated cone at the other. A pressure cell assembly is placed between the truncated surfaces and uniaxial compressive stress generated by a hydraulic press is applied to the ends of the carbide cylinders.

The area of the truncated surface determines the maximum mean pressure attainable by the anvils. Due to the relatively higher pressure experienced by the anvil surface with respect to the other end the differential shear forces developed would shatter it prematurely were it not for the 75° slope of the cone with respect to the cylindrical axis. This large angle gradually relieves the differential shear stress by distributing it over a larger and larger area and is the basis for the principle of "massive support", permitting the anvil surface to withstand several times its normal yield stress. The holes in the circular steel blocks are also machined to have a 1° taper but are 3 mils smaller in diameter than the carbide pieces. When the carbide pieces are forced into their steel "jackets" they experience a radial compressive stress which reinforces them and enables them to withstand higher axial compressive stresses. When the anvils are compressed the radial shear stress first cancels out the compressive stress developed by the steel jackets. Further axial compression changes the net radial stress into tensile but this destructive radial expansion is limited by the hoop tension developed in the steel jackets. Ideally, therefore, the maximum pressure that can be attained is limited by the hoop-tension strength of the steel jackets. In practice, however, the anvil surfaces undergo plastic deformation long before the calculated strength of the steel jackets is reached. These plastically deformed anvil

surfaces alter the pressure distribution within the pressure cell and change the load/pressure relationship in such a manner that eventually the rate of plastic deformation exceeds that of simple compression and little advantage is gained by further loading of the anvils. Another limiting factor is present when the limiting thickness of the pressure cell assembly is reached. If compression is continued, the anvils eventually rupture. The anvils used in these experiments had a surface dismeter of 1/2 inch and had a practical pressure limit of about 150 kbars when new. Larger cone slopes, smaller anvil area, and multiple jacket prestressing can produce pressures in excess of 200 kbars.

The uniaxial compressive stress is transformed into quasi-hydrostatic pressure when the sample is enclosed in a pressure cell (Fig. 5), consisting of a pressure transmitting "fluid" and a vessel containing this "fluid". Specifically, the sample is in the form of a thin wire sandwiched between two silver chloride discs 7 mils thick and just under 5/16 inch in diameter. The silver chloride discs were coated with a thin layer of acrylic paint to prevent corrosion of the sample wire. They are contained by two 10 mil thick pyrophyllite gaskets 3/32 inch wide and 1/2 inch in external diameter. Pyrophyllite ($Al_2Si_4O_{12}H_2$) is a volcanic lava rock which is highly compressible and has very high internal friction, i.e., shear strength due to its microcrystalline structure. Finely divided iron oxide (Fe_2O_3) powder is painted on the pyrophyllite gasket surfaces to increase the friction between the gaskets and anvil surfaces. When pressure is first applied, the gaskets, being some 5 mils thicker than the silver

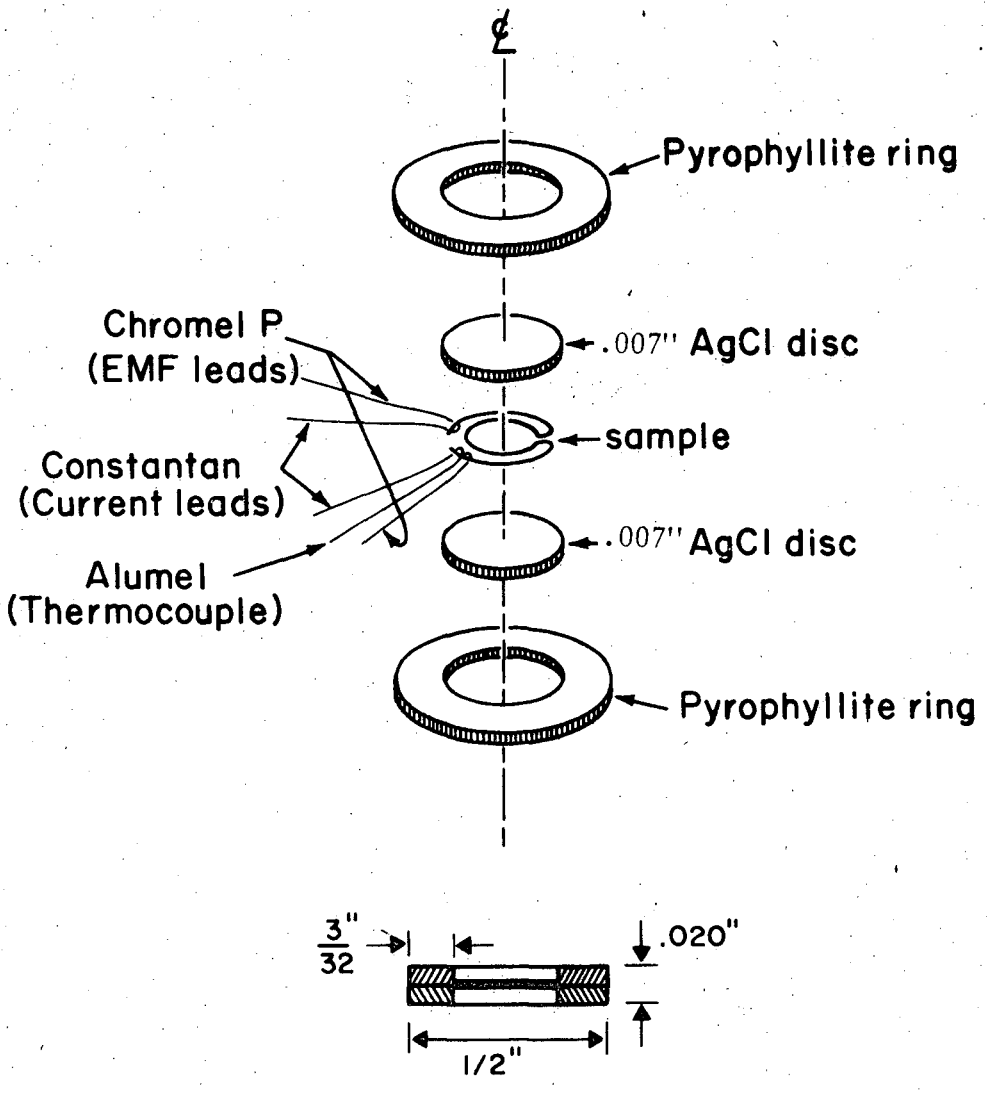

Fig. 5. Pressure cell assembly

chloride sandwich, receive all the load and are compressed until they are of the same thickness as the silver chloride sandwich. During this process the shear strength of the pyrophyllite rings is greatly increased and it is by virtue of this prestressing that they are able to prevent the subsequent tendency of the silver chloride to extrude through them and to increase the degree of hydrostaticity by simulating the rigid wall of a cylinder. (Experiments using silver chloride nearly as thick as the gaskets consistently resulted in "blow-out"). Continued compression applies pressure to both the gaskets and the silver chloride. As the silver chloride receives compression it at first expands in a radial direction until it fills up all the space surrounding it. When radial expansion is stopped by the pyrophyllite rings the low shear strength of the silver chloride enables pressure in the radial direction to develop and the wire sample begins to experience quasi-hydrostatic pressure. If the silver chloride had no shear strength, i.e., a perfectly non-viscous fluid, the sample would be under true hydrostatic pressure just as if it were in a piston-cylinder system. As it is, the pressure is never quite hydrostatic and furthermore this viscoelastic medium requires a finite period of time to approach an equilibrium. The virtue of the Bridgman opposed-anvils system lies in its ability to reach relatively high pressures, its ease of construction and its low cost. Despite its inability to produce truly hydrostatic pressures it nevertheless approaches it. Better static high pressure devices in terms of higher hydrostaticity and larger sample volume are the girdle and belt type divices and the multiple anvil devices. They are available at various degrees of higher initial cost and increased complexity.

The sample was in the form of a wire. Experiments with wires of various sizes indicated that because of the more favorable bulk to surface ratios, wires of larger diameters have a smaller percentage heat leak than those of smaller diameters. However there is a limit to the diameter of the wire because the presently available sensitivity requires a sample with as large a resistance as possible. The sample wire was 0.005 inch indiameter, nominally 99.99% pure, supplied by California Fine Wire Company, and annealed at 600°C for 12 hours in an argon atmosphere and cooled slowly. To obtain the maximum possible length, the wire was bent into a horseshoe shape (See Fig. 6). The circular shape of the sample was necessary to avoid a radial pressure gradient which exists in this geometry. Electrical leads must be attached to the sample for delivering the electrical current and measuring the voltage drop. These leads must be mechanically strong enough to withstand the severe shear stress that exists at the edge of the cell, sufficiently ductile so that they can be crimped onto the sample, and they must be poor thermal conductors to minimize heat leak. Since it is necessary to know the temperature of the samples, thermocouple wires must also be attached to it. Advantage was therefore taken of the fact that thermocouple wires often have the desired mechanical and thermal properties, and they were used as both the electrical leads and the thermocouple leads. The current leads were made of 0.005 inch constantan and the voltage leads 0.005 inch chromel P. Another 0.005 inch alumel lead was placed between one pair of constantan and chromel leads. The small section of iron wire between the chromel and alumel leads served as the junction, thus the detection of the true temperature of the sample was assured. The

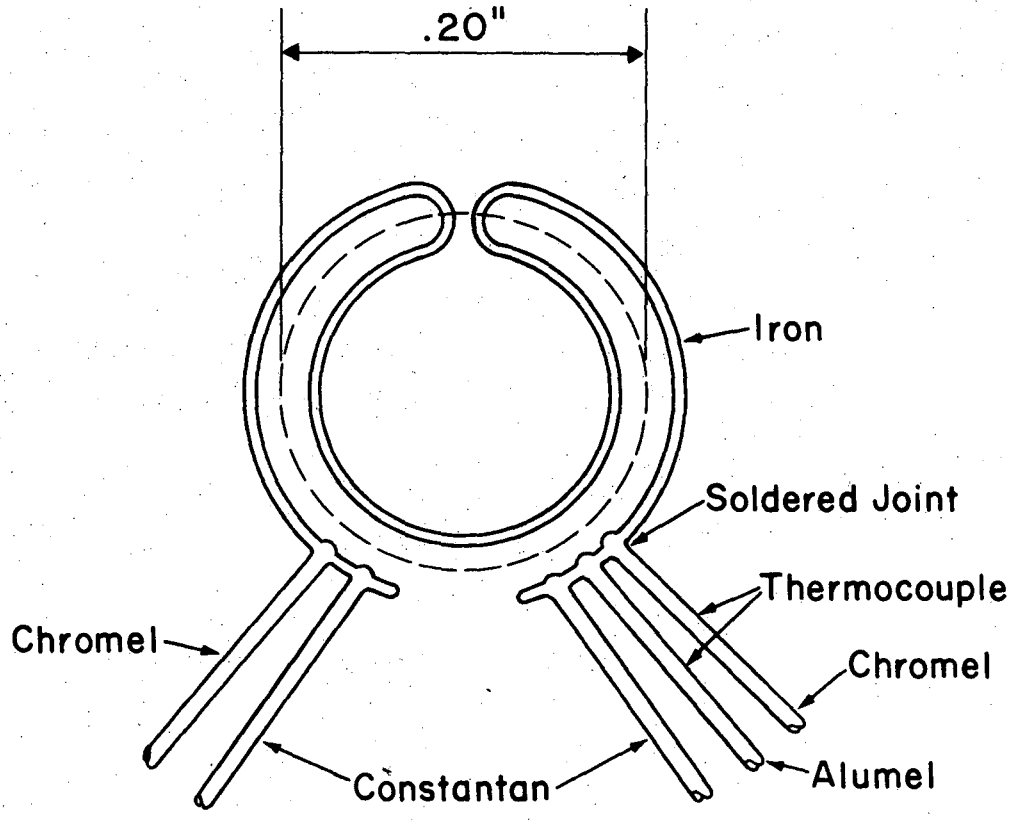

Fig. 6. Sample Wire and Leads

reason chromel was chosen as the voltage leads is because it has relatively small thermal EMF with respect to both iron and the brass binding posts of the measuring potentiometer. To ensure good electrical contact the ends of the leads were flattened, bent around the sample, crimped, and soldered. To prevent corrosion the entire sample-lead assembly was coated with a thin layer of clear acrylic. The leads were taken out of the pressure cell between the two AgCl discs and the two pyrophyllite gaskets. Larger gauge wires of similar materials were connected to these thin wires immediately outside the anvils.

Bismuth phase transitions at 25.4, 26.9 and 81[†] kbar were used to calibrate the pressure in the geometry of the sample. A 200 ton load cell in conjunction with a Baldwin-Lima-Hamilton Type 20 Strain Indicator were used to monitor the load applied to the anvils. A lienar load-pressure relationship was assumed for interpolation between 25 and 81 kbar. The pressure scale is estimated to be accurate to ± 5%.

B. Constant Current Pulse Generator

One of the most important requirements of the pulsing technique is that the current pulse be constant. At the end of a one millisecond pulse, the resistance change is often only a few percent;

[†] The 81 kbar (III-V) transition was obtained by pulsing the Bi calibration sample with the constant current pulse generator described in the next section. The thermodynamic value for this phase transition is generally taken to be 81 ± 3 kbar.

therefore a current pulse that is constant to only one percent can contribute a very significant error. To minimize this source of error, the current pulse must be constant to the order of a hundredth of a percent. Since the heat leak during the pulse becomes significant after approximately 500 microseconds, the current must be able to reach within a few hundredth of a percent of the final value within a fraction of this time so that meaningful results can be taken before the heat leak renders the data extremely difficult to analyze. Clearly a mechanical switch or even a electro-mechanical relay cannot provide a clean, noiseless pulse on such a short time scale. A solid state switch provides the obvious solution. However, when attempts were made to switch constant current supplies that were commercially available and otherwise met the ripple, noise and regulation requirements, either "ringing" persisted for a least 200 microseconds, or a high frequency oscillation took place throughout the pulse. These commercial power supplies were designed for stable operation and not for dynamic load changes, and were not suitable for these experiments without major modifications. A constant current pulse generator, as a consequence, had to be designed by the author.

A detailed description of this pulse generator appears in Appendix I. It has a maximum output of 10 amperes with a compliance voltage of 15 v. Pulse duration is variable between 100 microseconds and 500 milliseconds. The current pulses are estimated to be constant to better than ±.05% and the rise time is typically 25 microsecond to within 1 ma. of the final value.

The magnitude of the current pulse appears in the third power in the expression for C_p; errors in measuring them therefore are magnified approximately three times. Thus it is essential to be able to measure the current with as small an error as possible. Because of the short duration of the current pulse no commercially available test instruments are available to measure it with sufficient accuracy and resolution. Accurate measurements were made possible by an Analog Divices Model 350B Comparator which has one of its inputs connected to the current sensing shunt R_i and the other input connected to a Lambda Model LS511 precision voltage source capable of delivering 10 volts with a resoltuion of .1 mv. Whenever the pulse voltage equals or exceeds the preselected voltage on the Lambda a pulse appears at the output of the Comparator which is observable with an oscilloscope. (See Fig. 8). Resolution of 1 ma. can be achieved. The current pulses used in these experiments were typically several amps so and uncertainty of 1 ma. represented less than .1% error. In fact for currents larger than 3 amps the error in I^3 was equal to or less than 0.1%.

C. Resistance and Temperature Measurements

The resistance of the sample was measured by passing a constant current through it and the potential drop measured with a potentiometer. The current, which was constant to 0.01%, was measured by passing it through an N.B.S. standardized 1 ohm resistor and the voltage drop first measured by a potentiometer and then constantly monitored with a Fluke differential voltmeter which had adequate stability and resolution. The potentiometer used was a Leeds and Northrop K-3 Universal Potentiometer. All resistance measurements were made with

the current flowing in both directions to eliminate spurious and thermal EMF. Contact resistance was eliminated by virtue of the four-lead sample used. Resistances ranged from several tens of milliohms to tenths of ohms. The current used was 100 ma. throughout the experiments. Accurate measurement of 10 μohm was possible. Joule heating, which amounted to a maximum of several milliwatts, had negligible effect due to the intimate contact between the sample and the silver chloride.

Measurement of the true temperature of the sample was possible because the sample itself formed part of the thermocouple junction. The chromel-alumel thermocouple was calibrated, with its reference junction in an ice-water bath, in CO_2 solid-vapour bath in a manner recommended by Ref. 32, and in O_2 liquid-vapour bath. The liquid oxygen was obtained from the Giauque Low Temperature Laboratory of the University of California, Berkeley. Secondary calibration was also made with fresh liquid nitrogen, although the results were inconsistent. Pressure effects were corrected according to the results published by Bundy.[33] The thermocouple table published in Ref. 34 was used for interpolation. The thermocouple E.M.F. was measured with a White double potentiometer. It was felt that the temperature measured was accurate to .1°.

D. Measurement of dE/dt

In principle dE/dt could be measured by displaying the pulse of the voltage drop across the sample on the screen of an oscilloscope and then recording the image with a camera. In practice the fact that the resistance was changing with time was completely masked by the relatively large magnitude of the voltage pulse. A pulse consisted

of a flat part equal to IR_o and a part resembling a right triangle with the slope of the hypotenuse equal to dE/dt (Fig. 7). IR_o was typically a few hundred mV and the slope typically a few mV per μsec. Obviously the slope could be increased by increasing the current I. Maximum I was limited by the output power capability of the current pulse generator and the 10v. output limit of an amplifier used to amplify the voltage pulse. With a gain of 10 in this amplifier the maximum signal that could be amplified was 1 volt. If this amplifier was not used the long cables between sample and electronic instruments picked up 60Hz and sometimes even radio frequency noises which drastically reduced the signal to noise ratio. Furthermore increasing the current compounded the problem of looking at a still relatively small dE/dt on top of an increase IR_o. In principle, this problem was solved ingeniously by Stark.[16] If it was somehow possible to reject the IR_o part and observe only the right-triangular part on the oscilloscope the entire screen area could be utilized and a large, measurable slope could then be photographed. A Tektronic Type W plug-in amplifier was used for that purpose. This author found, however, that the Type W produced distortions when the highest sensitivities were used (see Appendix I). Besides, the manner in which the Type W was used by Stark did not measure the true voltage drop across the sample but instead measured the total voltage drop between the switching transistors, the sample, the current leads and ground.

In these experiments the IR_o part was subtracted from the total pulse by using an arrangement of three amplifiers (see Fig. 8). The preamplifier A, a Burr-Brown Model 3061/25 instrumentation amplifier,

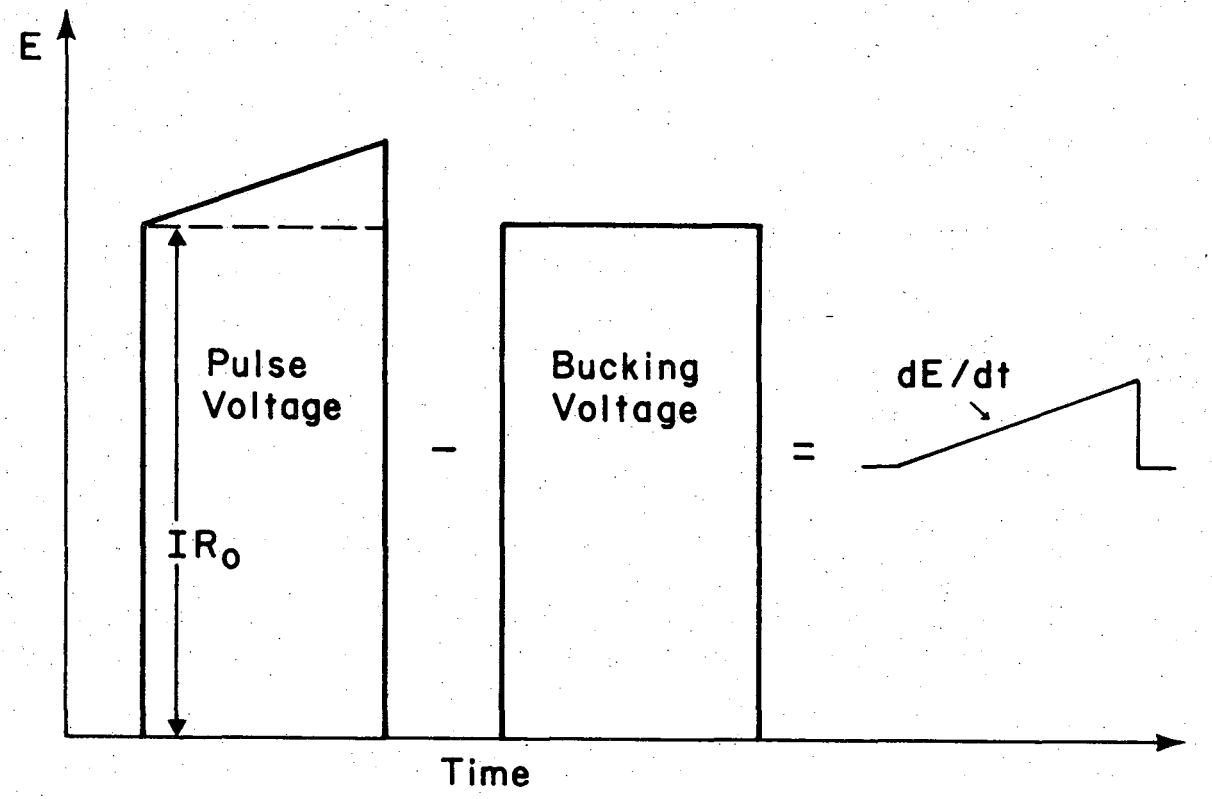

XBL 7110-7448

Fig. 7. Schematic illustrating the method used to separate a small $\frac{dE}{dt}$ from a large voltage pulse.

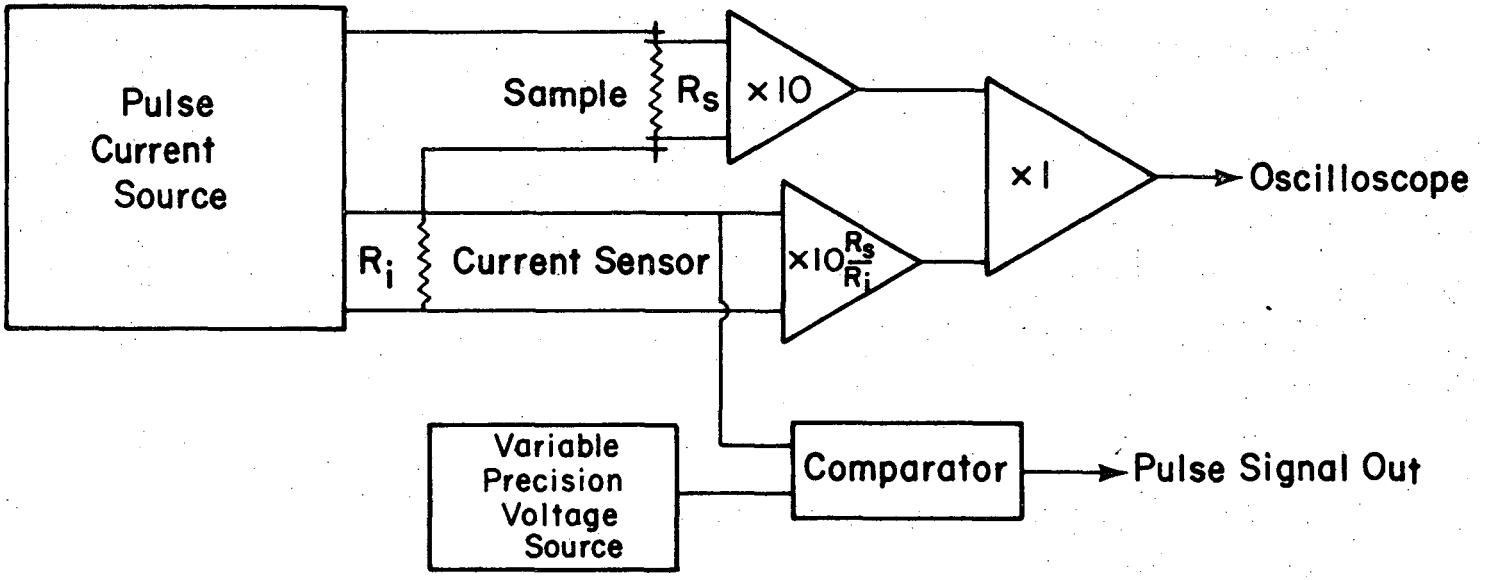

XBL 711-6439

Fig. 8. Block diagram of the instruments used for amplifying $\Delta E(t)$ and for measuring the current.

was set for a gain of 10 and placed physically as close as possible to the sample. Output of this amplifier was sent into one input of a differential amplifier B, a Burr-Brown Model 3061/16 instrumentation amplifier. A variable gain amplifier C, constructed from an Analog Devices Model 148B fast-settling operational amplifier, amplified the voltage drop IR_i across the current sensor R_i inside the pulse current generator by a factor of $10 \times (R_o/R_i)$. Its output, which is always equal to $10\ IR_o$ irrespective of the value of I, was then sent into the other input of amplifier B. Out put of amplifier B thus equalled to $10(IR-IR_o)$. The advantage of this system was that other than the fact that it did not have the distortion of the Type W, once the correct gain for amplifier C was set according to a given R_o, a series of differnet current pulses could be pulsed through the sample and the results recorded on the same photographic film which only exhibited the change in E, greatly saving time and effort which was important during an isobaric run when the temperature was rising rapidly.

The slope of the traces on the photograph was measured with a direct reading slope measuring device with a theoretical resolution of better than 0.1%. This was, however, not the limiting factor due to the fact that the traces had finite width and contained random noise (see Fig. 9). The random noise effect was minimized by exposing the same pulse several times rapidly. The slope was then measured several times and the average deviation of the results was not more than 2%. The most serious problem encountered was that of the reactance presented by the sample and lead geometry and the fact that the sample had a small resistance.

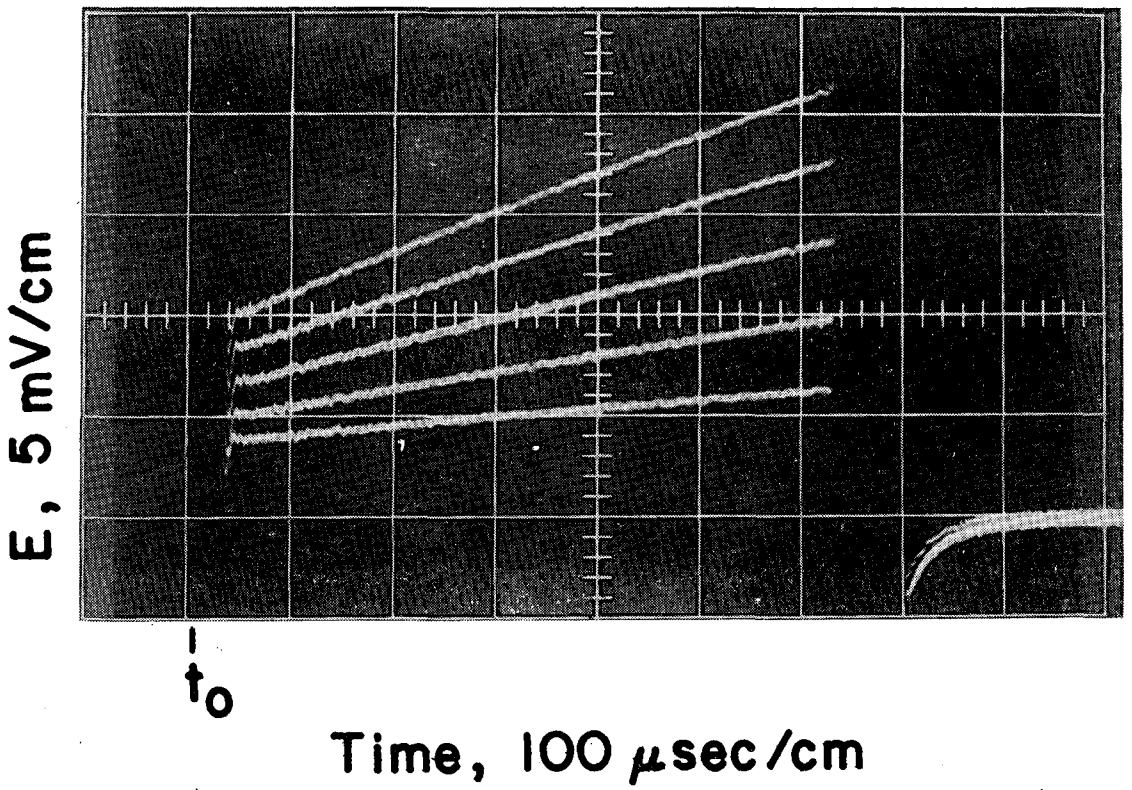

Fig. 9. Typical photograph of pulses.

IV. RESULTS

After the sample and pressure cell had been assembled on the surface of the bottom anvil, the top was carefully lowered onto the bottom one with the aid of an aligning device. The entire assembly was then clamped tightly and carefully placed in a cylindrical stainless steel can with polystyrene foam insulation on the outside. The steel can was open at one end and was used as a container for the coolant and "heat sink". The can was then placed on the ram of the hydraulic press and laminated fiber-glass epoxy blocks were used to insulate the can from the press. The remaining space between the top of the back-up block and the frame of the press was filled with steel blocks. (Fig. 10) Pressure was slowly applied until good thermal contact between the sample and the AgCl discs had been established. This was evidenced by a significant change in the heat dissipation rate from the sample when long current pulses (5 msec.) were applied. This was achieved at a pressure of roughly 1 kbar.

When it had been established that the sample was good and all the electrical signals appeared normal copper rods 3/4 inch diameter and 9 inches in length were strapped securely around the anvil assembly and the back-up blocks. Two additional layers of copper rods were then strapped around the first one. A total of approximately 150 lbs of copper was used for this "heat sink". To provide faster warming rates a heating tape connected to a Variac was wound around the copper rods. For each isobaric run the pressure was increased at room temperature to the desired value. The steel can was then filled with liquid nitrogen. As cooling progressed a constant load was

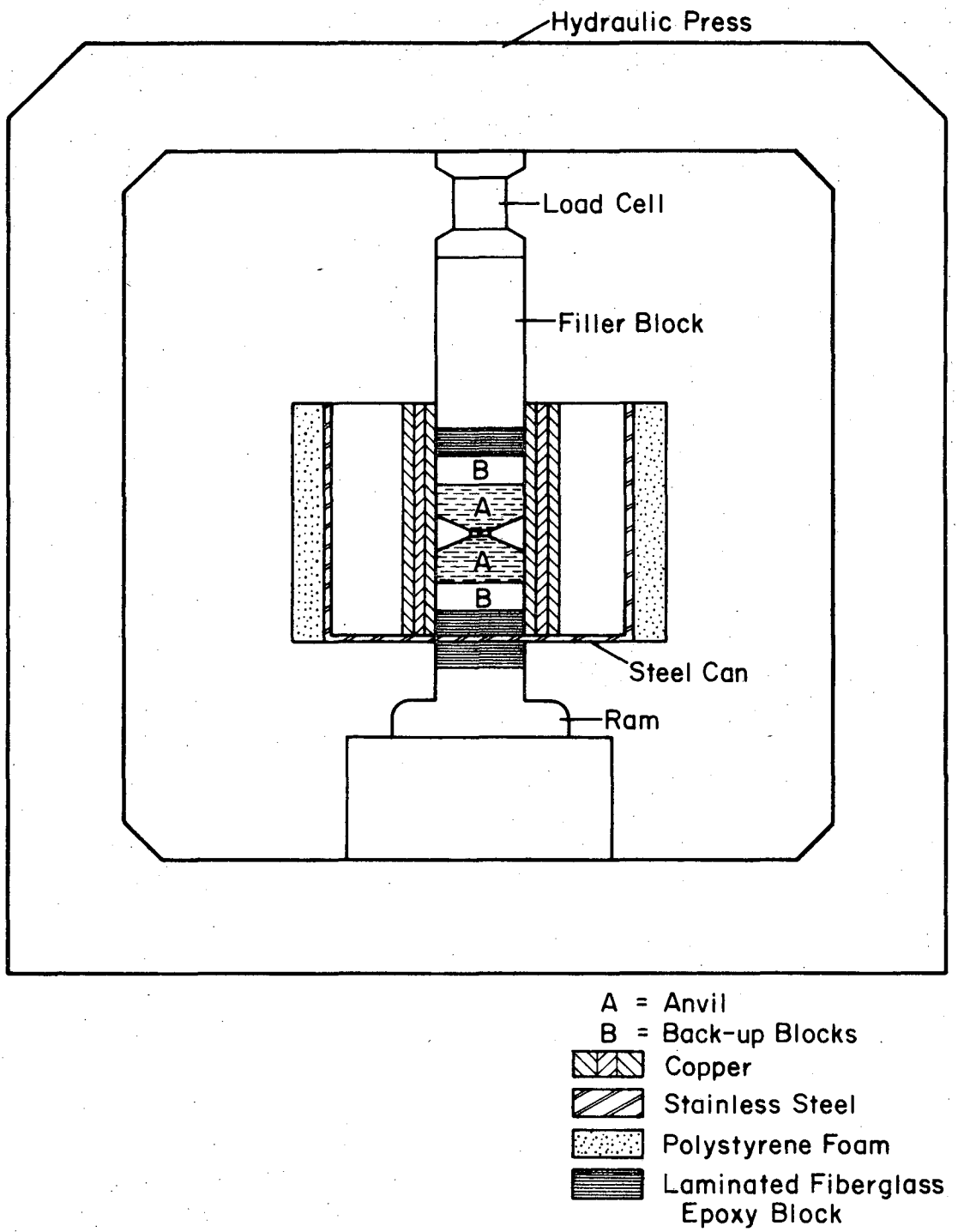

Fig. 10. Experimental Set-up

maintained so that the pressure would not be reduced because of thermal contraction. It is usually assumed in high pressure research that by maintaining a constant load the pressure remains constant.

Owing to unavoidable heat transfer between the steel can and the press, the system (the system here is arbitrarily defined as the sample, pressure cell, anvils and the copper rods) reached a steady state at 83°K. When all the liquid nitrogen boiled off, the temperature of the system increased rapidly at a rate of approximately 0.3° per minute. At about 100°K the warming rate decreased to approximately 0.2° per minute, which rate persisted until almost 200°K, at which point the heating tape was turned on to maintain this rate. Again the load was maintained at a constant value to avoid increased pressure from thermal expansion. Each of the isobaric runs was terminated at 274°K and lasted approximately 24 hours.

A total of five isobars at 1, 25, 35, 45, and 75 kbar were determined. The same sample was used for all the runs. The pressure for the 1 kbar run was uncertain because in the Bridgman anvil system any pressure below 20 kbar is unreliable. In this range the AgCl has not reached the "fluid" state, hence it is not a "good" pressure transmitting fluid. This fact becomes obvious when one compares the resistance vs. pressure curve obtained in a more nearly hydrostatic system with a typical curve obtained in the present pressure system. (Fig. 11) It can be seen that the curves are quite similar after 25 kbar. For this very reason, the C_p data for the 1 kbar run will merely be used for comparison with existing calorimetric data and will be excluded from equation of state calculations. The variation in C_p between 25 and 45 kbar was so small that an additional run at

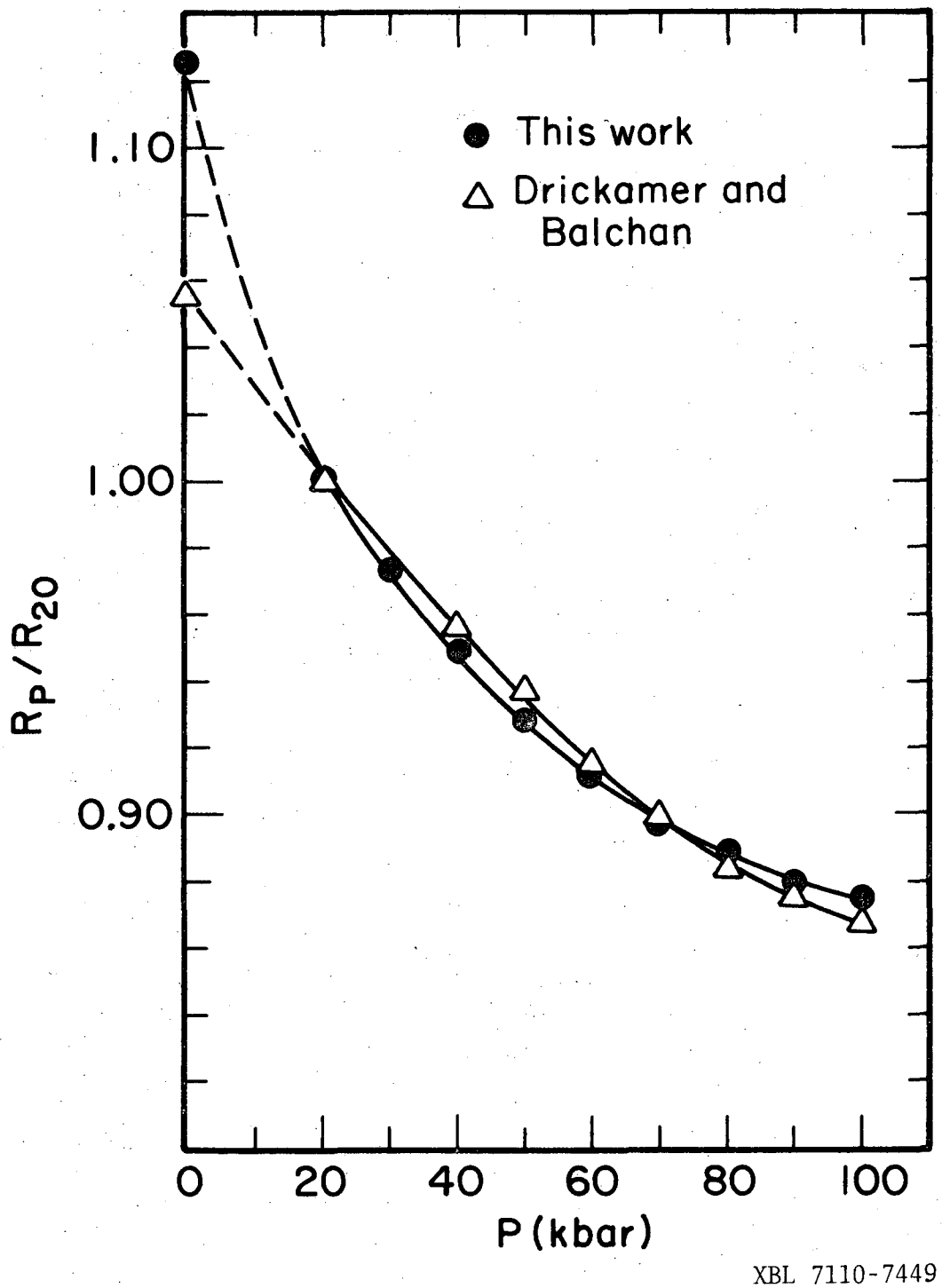

Fig. 11. Reduced resistance vs. pressure for iron.

75 kbar was considered sufficient to represent the C_p vs. P relationship in the b.c.c. phase. An attempt was made to measure the C_p in the h.c.p. phase but the anvils ruptured at 110 kbar. The experiment was terminated at this point.

Resistance and temperature were measured at 1° and photographs of pulses for C_p at 5° intervals. Each photograph recorded four to five pulses at different currents. The currents were chosen so that the maximum power output was utilized and that the minimum slope was 20%. All measurements were taken as function of time. The time resolution was 0.1 minute.

The resistance and temperature data were plotted against time and smooth curves were drawn through the points. At no time was the thermal EMF in measuring resistance larger than 0.1% of the total voltage. Figure 12 shows some typical R and T vs. time data. Resistance values were read off these smooth curves at one degree intervals and again plotted. Figure 13 shows the smooth curves of R vs. T for all the isobars.

R' was calculated by using a combination of numerical and graphical methods: $(R_n - R_o)/n$ were calculated at 5 degree intervals, n being the number of 1 degree increments, the maximum being five; and R_o the resistance at the temperature where R' was desired. The calculated $(R_n - R_o)/n$ were then plotted and smooth curves drawn through them to obtain R'. Figure 14 shows smoothed R' vs. T for all the isobars. R' was not calculated for both ends of the isobars because of the inherently unreliable results one could obtain in those areas in numerical differentiation. Usable results between 110 and 260°K were calculated. The error in calculating R' is probably 1%.

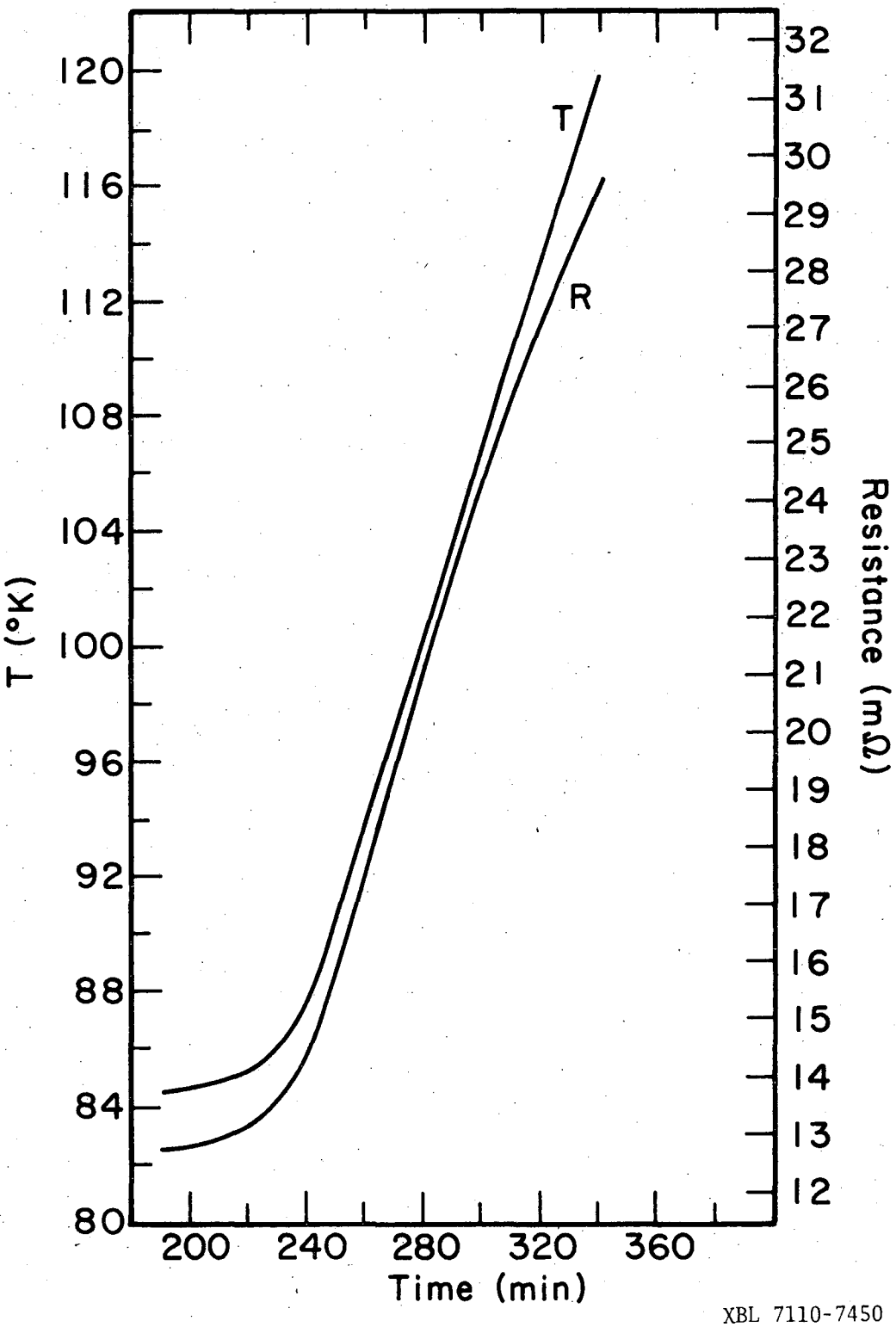

Fig. 12. R and T vs. Elapsed Time Curves.

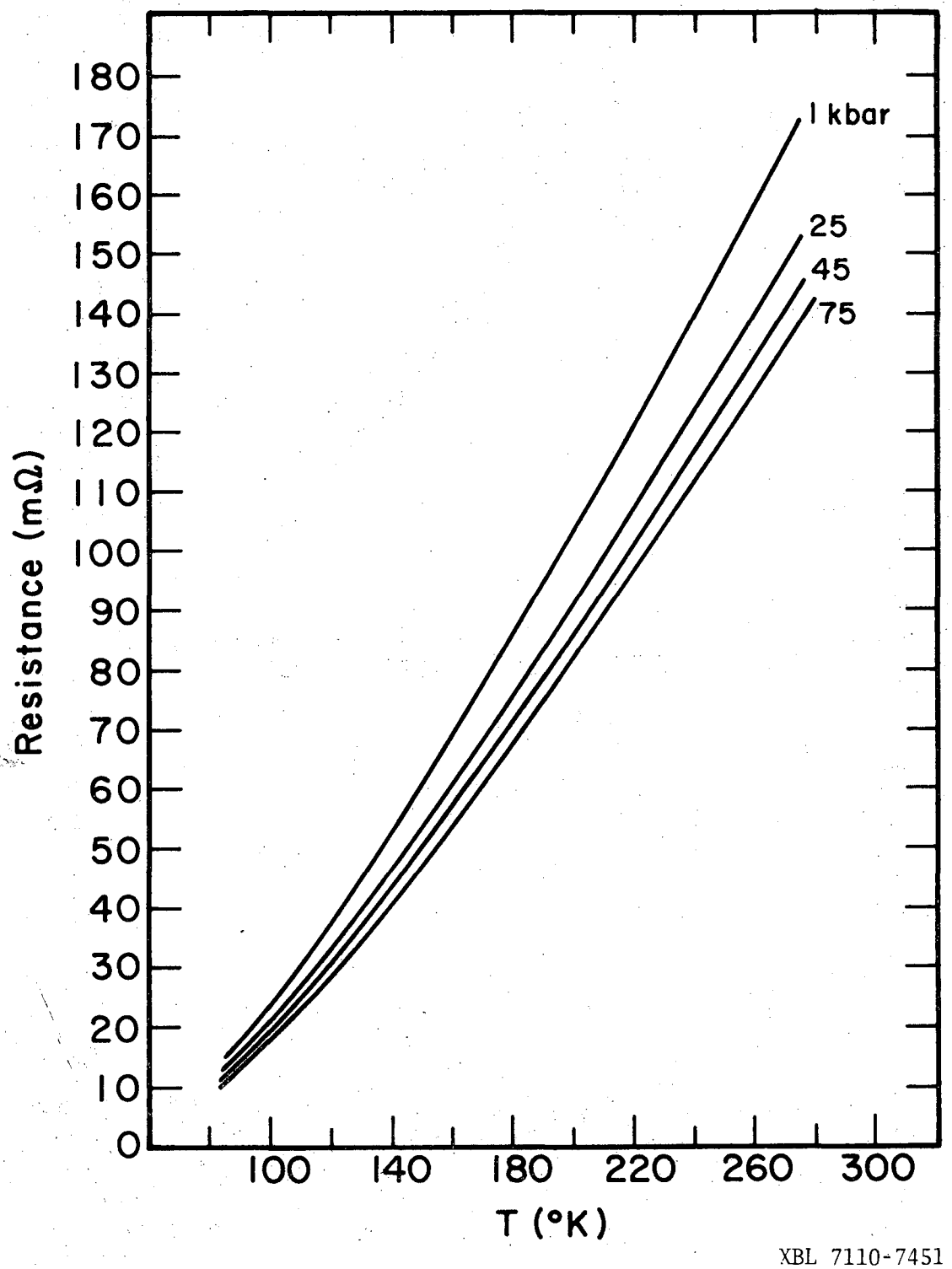

XBL 7110-7451

Fig. 13. R vs. T Isobars of Iron

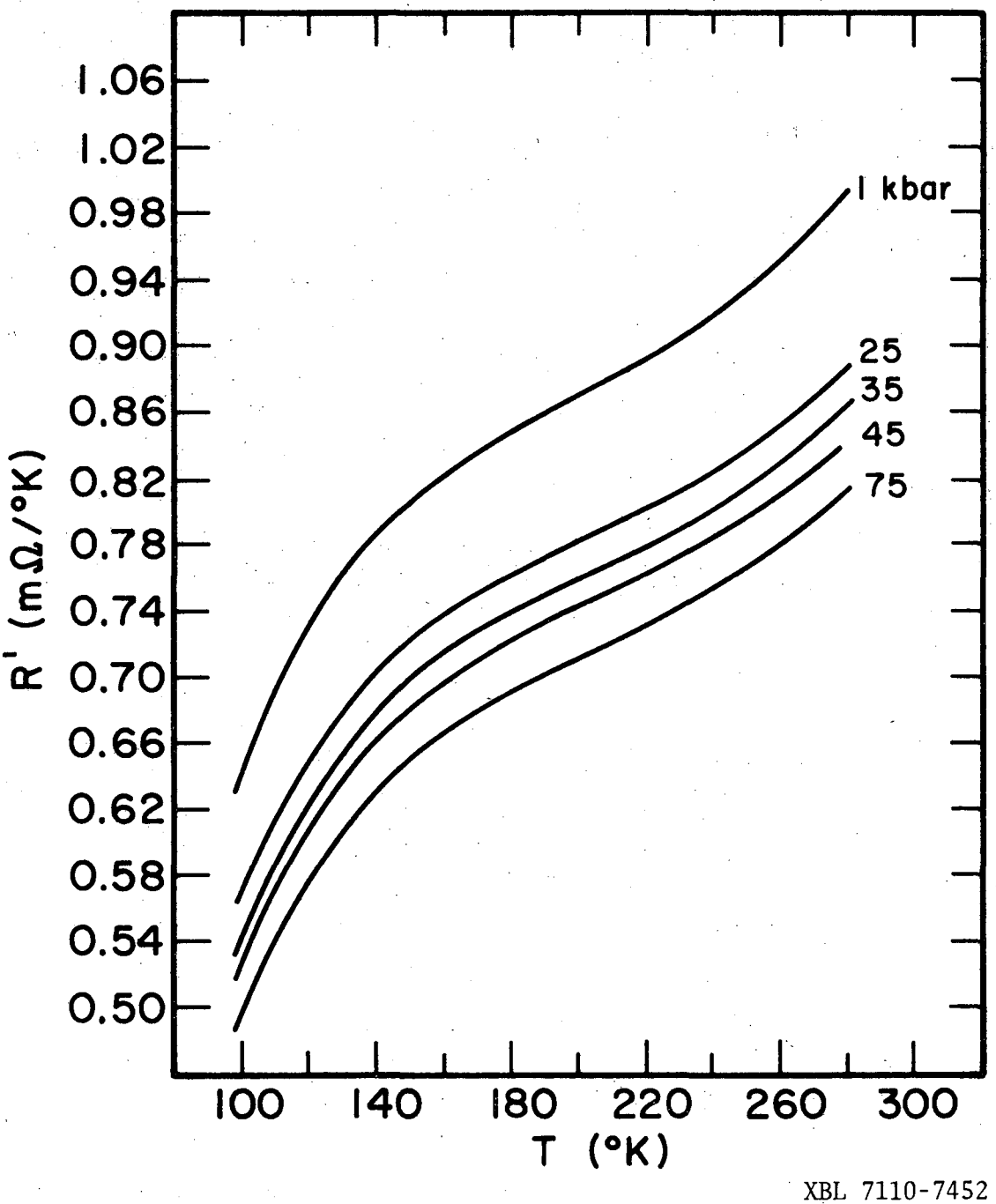

Fig. 14. R' vs. T Isobars of Iron

It has been pointed out in Section C of Theory that if the $\frac{1}{I}\frac{dE}{dt}$ vs. I^2 plot shows zero intercept then the effect of heat leak can be ignored. This result was obtained in all photographs except those taken at temperatures below 110°K. Figure 15 illustrates some typical results when $\frac{dE}{dt}$ is plotted against I^3. The average error in measuring the slope is 2%. The error could be as high as 3% for the low temperature points due to smaller slopes. It required experience in choosing the part of the photographed trace which was relatively immune from both the non-ideal behavior of the electronics and the heat leak. The same set of criteria was consistently used throughout the measurements.

We now compare the 1 kbar C_p result with the one atmosphere C_p obtained by Kelley[35] using calorimetry. Since the 1 kbar data are in arbitrary units, a numerical factor is calculated from the average of the ratios from the two sets of data. When all the proper adjustments are made we find the two sets of data in much better agreement than the estimated 3% error in the high pressure data. In Fig. 16 we show the percentage deviation from Kelley's data vs. temperature. The smoothed data are represented. At 1 kbar the volume of iron has decreased less than 0.1% (Fig. 1); we expect the heat capacity to be substantially the same as it is at one atmosphere. The agreement is rather remarkable.

We show in Fig. 17 C_p for 25, 35, 45, and 75 kbar. Except for the 25 kbar one all the curves have been displaced by 70°K from each other. If we draw the curves without displacing them they are difficult to differentiate from each other, and one is tempted to conclude that within the estimated 3 to 4% error the heat capacity does not change from 25 to 75 kbar. This would be a reasonable

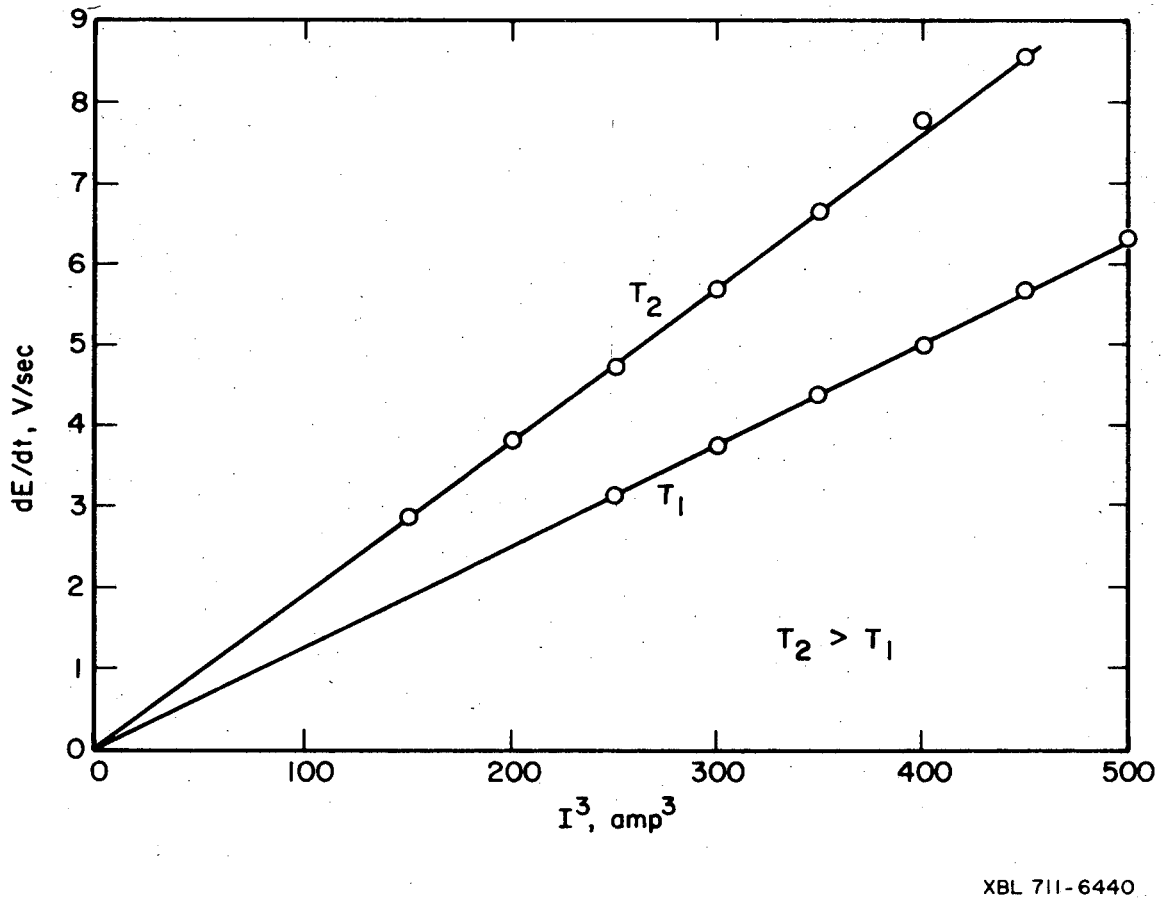

Fig. 15. Typical $\frac{dE}{dt}$ vs. I^3 plot for two temperatures.

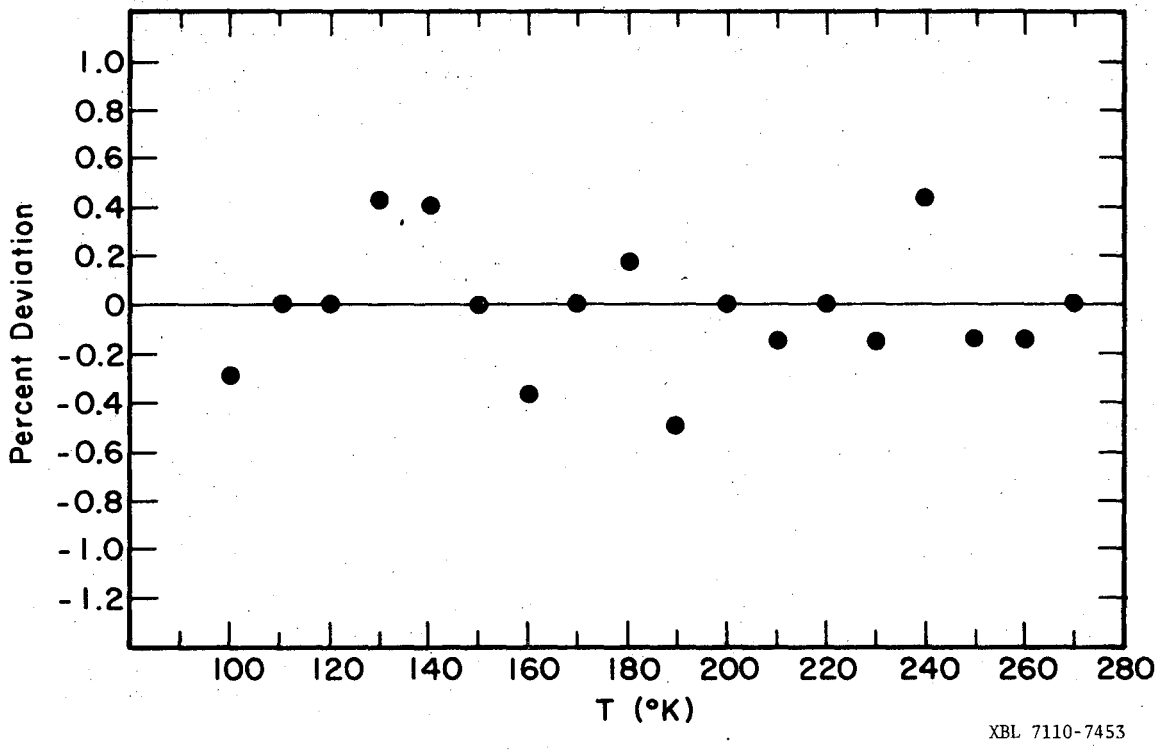

Fig. 16. Percentage Deviation of 1 kbar C_p of iron from Kelley's Data

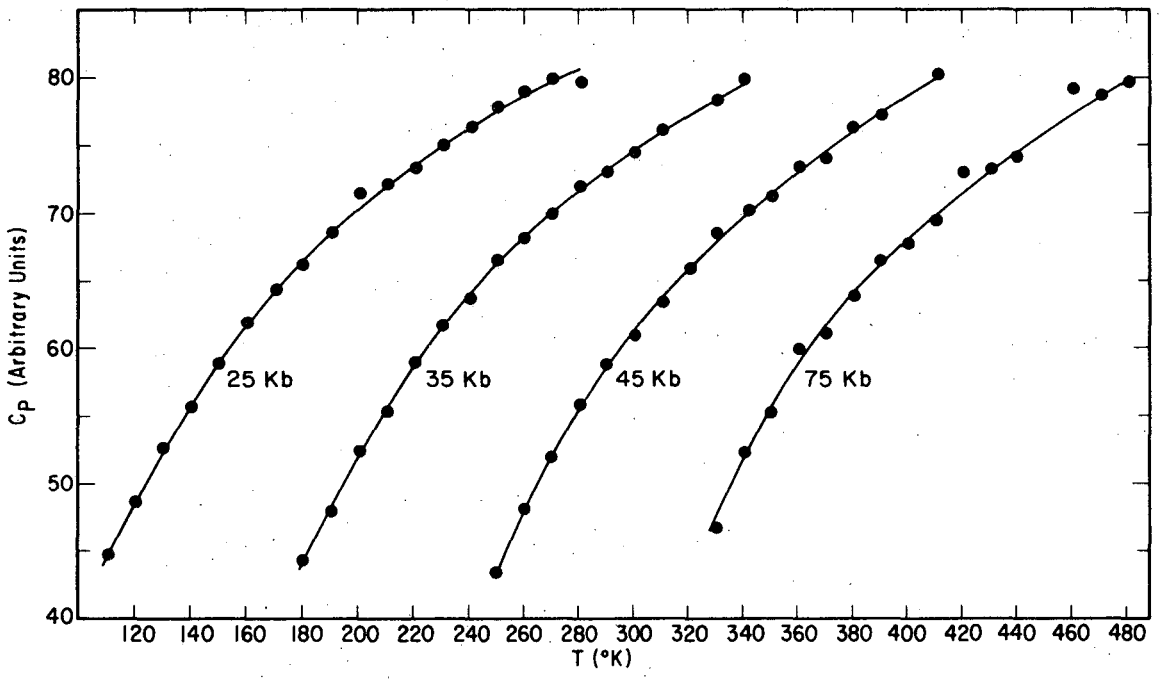

XBL 7110-7454

Fig. 17. Heat Capacity Isobars for Iron

enough conclusion. But careful examination of the data reveals a slight decrease with pressure along the isotherms. We shall now investigate this decrease and compare it with existing data.

We take the data along the isotherms and perform least squares fits to the equation

$$C_p(T,P) = C_p(T,0) + \left(\frac{\partial C_p}{\partial P}\right)_T P \qquad (34)$$

and plot the calculated $\left(\frac{\partial C_p}{\partial P}\right)_T$ from the smoothed data in Fig. 18. We find that most of the $\left(\frac{\partial C_p}{\partial P}\right)_T$ are negative and tend toward zero as the temperature increases, which is consistent with theoretical predictions.

We now compare $C_p(T,0)$ calculated from Equation (34) with Kelley's data. Again we calculate a factor from the average of the ratios between the two sets of data. In Fig. 19 we again plot the percentage deviation from Kelley's data against temperature and it can be seen that although the deviation is somewhat systematic at different portions of the plot the average deviation is only 0.5%.

If we now draw the best straight line through the points in Fig. 16 and use the points on this line to calculate the change in Θ_D, assuming that $\Theta_D = 432°K$ at one atmosphere, we find that Θ_D has increased between 4 to 5 degrees in going from 25 to 75 kbar. Assuming that Grüneisen's constant has not changed from its one atmosphere value of 1.7 and knowing that the volume has decreased by 2.5% from 25 to 75 kbar (Fig. 1), we get from Equation (15) an increase in Θ_D by 18 degrees. Given the large scatter in the points presented in Fig. 18 this poor agreement is not surprising.

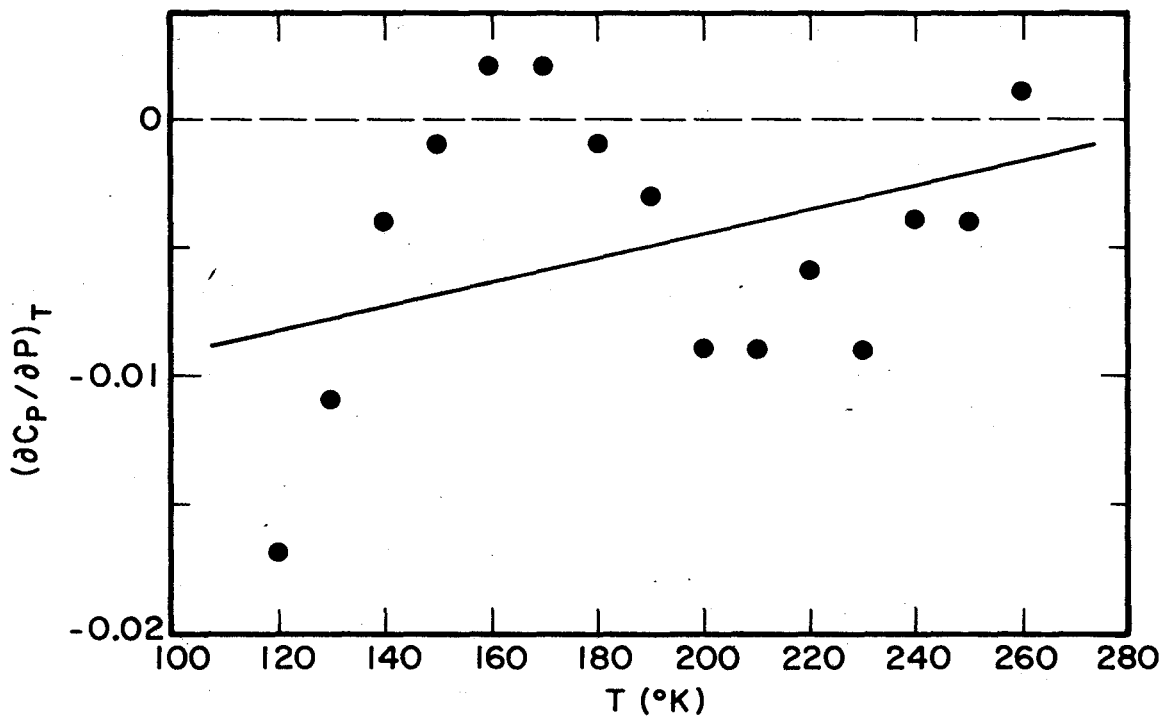

XBL 7110-7455

Fig. 18. $\left(\frac{\partial C_p}{\partial P}\right)_T$ vs. T calculated according to Eq. (34)

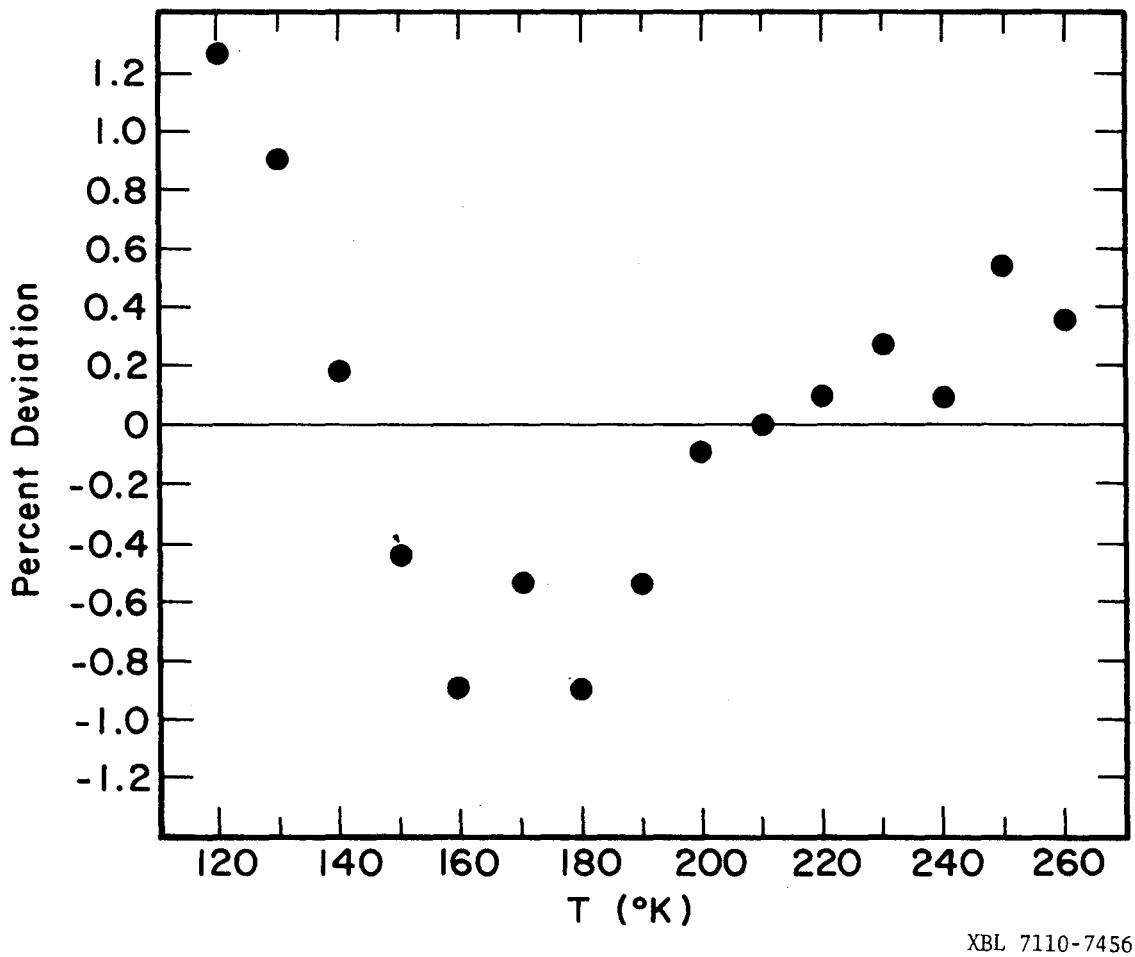

Fig. 19. Percentage deviation from Kelley's data for 0 kbar C_p calculated according to Eq. (34).

Nix and McNair[36] have measured the thermal expansion of iron at one atmosphere. It is possible to estimate $(\partial^2 V/\partial T^2)_P$ from their data. If it is assumed to be constant with pressure one would get a decrease of approximately 2.5% in C_p at room temperature in going from 0 to 75 kbar. Our data shows a decrease of perhaps .2%. Again the agreement is poor, although the 2.5% change is certainly within our experimental error.

Finally, the γ calculated is 0.45. So the equation of state is

$$P = \frac{-dE_o}{dV} + \frac{0.45}{V}(E - E_o) \qquad (35)$$

V. DISCUSSIONS AND CONCLUSION

The results we have obtained thus far are puzzling. The remarkable agreement between the 1 kbar data, the extrapolated 0 kbar data and Kelley's one atmosphere calorimetric data is reassuring and lends credence to the instruments and methods used in this work. In view of the preceding the discrepancy between our results and those calculated from Grüneisen's constant and thermal expansion data is somewhat perplexing even though there is some uncertainty in the previous work.

In calculating $(\partial C_p/\partial P)_T$ we have only four points for each isotherm, which is not sufficient to accurately define a slope. The scatter in Fig. 18 makes this point abundantly clear. We have also assumed that $(\partial C_p/\partial P)_T$ is not dependent on pressure, which is probably not rigorously true, but our data do not permit a more refined analysis. It is also possible that non-hydrostatic stress exists in the pressure cell. In developing quasi-hydrostaticity in the Bridgman anvil system, there is an implicit assumption that the sample's dimensions are small compared with the pressure cell, although no firm criterium exists. 5 mil wires have been used with apparent success in other experiments. The existence of non-hydrostatic stress can deform the lattice and therefore change the lattice vibration frequency spectrum. We must bear in mind, however, that heat capacity, being a macroscopic property, is not sensitive to minor local distortions. The distortion would therefore have to be extensive to affect the heat capacity. It is possible that as the pressure was raised beyond 1 kbar the non-hydrostatic stress gradually built up,

although samples that had been subjected to 25 kbar and taken out did not show any apparent signs of permanent deformation. Work is now underway in this laboratory to subject samples to various amounts of pressure and using X-ray to detect the presence of permanent strain.

Let us now examine the validity of the predictions based on Grüneisen's constant and the thermal expansion data. Grüneisen's constant is actually not exactly a constant. The assumption that all lattice modes change at the same rate with volume and that it remains constant has always been questioned.[37] In fact γ has been found to decrease with increasing pressure for most substances.[38] Therefore the prediction of an 18 degree decrease in θ_D is probably an over estimation; although it is not clear how this should be modified.

The thermal expansion data on iron by Nix and McNair[36] was obtained from a 99.99% pure sample. These authors pointed out that the thermal expansion coefficient for ferromagnetic materials is extremely sensitive to the amount and type of impurities present. Their data above 200°K differed considerably from some other works cited in their paper and showed an anomalous maximum at approximately 300°K which they attributed to impurities. It should be mentioned that their sample was the purest of all the works cited by them. While their data was sufficiently good to obtain the first derivative for the purpose of comparison with Grüneisen's law on thermal expansion, the accuracy of the second derivative is questionable. The author is not aware of the existence of more recent data on thermal expansion.

The questions raised here suggest methods to clarify them. To minimize the effects of non-hydrostaticity and heat leak, a piston-cylinder device where there is more sample volume could be used. A larger sample volume allows one to increase the sample diameter as well as its length. A belt type device, which also has larger sample volume, could be used to extend the temperature range to beyond iron's Curie temperature of 1043°K and the pressure range to over 200 kbar. This would allow one to measure the heat capacity of iron through the order-disorder as well as the crystallographic phase transitions. If longer sample wires can be used, then other materials that have low resistivity but high compressibility and Debye temperature could be used to investigate the equation of state. One metal that immediately comes to mind is aluminum which is highly compressible and has a Debye temperature of 430°K and has the advantage of being a simple metal.

The constant current pulse generator developed in this work can profitably be used in the determination of heat capacity of metals at high temperatures where the radiation loss of energy is a major problem when pulse heating is used. By virtue of its ability to generate very precise pulses of energy for durations as short as 100 μsec. the radiation loss could be minimized. It is a rather simple matter to modify this current generator so that it generates constant power at a small sacrifice in rise time and regulation. This modification could be used to measure for example the kinetics of solid-solid phase transitions under pressure.

To summarize, theories for the determination of equations of state of solids from heat capacity have been presented. The procedure

for measuring heat capacity under pressure has been described. A precision constant current pulse generator has been developed for the pulse heating method used. Heat capacity of iron has been measured from 110 to 260°K and from 25 to 75 kbar. An increase of 4 to 5 degrees in the Debye temperature is noted. Finally, the Grüneisen equation of state is calculated.

PART 1. REFERENCES

1. C. C. Swenson, Physics at High Pressure, in Solid State Physics, vol. 11, edited by F. Seitz and D. Turnbull (Academic Press, Inc., New York, 1960) pp. 41-147.
2. P. W. Bridgman, The Physics of High Pressure, (G. Bell & Sons, Ltd., London, 1949).
3. J. W. Stewart, Phys. Rev., 97, 578(1955).
4. See, for example, chapters by J. C. Jamieson and L. F. Vereschchagin, in Progress in very High Pressure Research, edited by F. P. Bundy, W. R. Hibbard, Jr., and H. M. Strong (John Wiley & Sons, Inc., New York, 1961).
5. R. L. Mills and A. F. Schuch, Phys. Rev. Letters 6, 263(1961).
6. F. J. Webb, K. R. Wilkinson, and J. Wilks, Proc. Roy. Soc., (London), A214, 516(1952).
7. J. S. Dugdale and F. E. Simon, Proc. Roy. Soc., (London), A218, 291(1953). See also E. C. Heltemes and C. A. Swenson, Phys. Rev. 128, 1512(1962).
8. G. Ahlers, Some Properties of Solid Hydrogen at Small Molar Volumes, (Ph. D. Thesis) UCRL-10757, Sept. 1963.
9. J. C. Ho, N. E. Phillips, and T. F. Smith, Phys. Rev. Letters, 17, 694(1966).
10. N. E. Phillips, private communication.
11. O. L. Anderson, Progress in Very High Pressure Research, edited by F. P. Bundy, W. R. Hibbard, Jr., and H. M. Strong, (John Wiley & Sons, Inc., New York 1961).

12. B. J. Alder, Physics Experiments with Strong Pressure Pulses, in Solids Under Pressure, edited by W. Paul and D. M. Warschauer, (McGraw-Hill Book Co., Inc., New York, 1963).

13. M. H. Rice, R. G. McQueen and J. M. Walsh, in Solid State Physics, vol. 6, edited by F. Seitz and D. Turnbull, (Academic Press, New York, 1964).

14. R. Grover, J. Phys. Chem. Solids, 31, 2347(1970).

15. D. Raimondi and G. Jura, J. Phys. Chem. Solids, 28, 1419(1967).

16. W. A. Stark, Jr., Thermal Pulsing of Metals Under High Pressure, (Ph. D. Thesis) UCRL-17454, April 1967.

17. D. C. Wallace, D. H. Sidles and G. C. Danielson, J. Appl. Phys. 31, 168(1960).

18. J. C. Slater, in Introduction to Chemical Physics, (McGraw-Hill Book Co., Inc., New York, 1939) Chap. 13.

19. C. W. Garland and G. Jura, J. Chem. Phys 22, 1108(1954).

20. T. H. K. Barron, Phil. Mag. (7), 46, 720(1955).

21. C. Kittel, Introduction to Solid State Physics, 3rd ed., (John Wiley and Sons, New York, 1966).

22. M. Blackman, The Specific Heat of Solids, in Handbuch der Physik, vol. 7/1, (Springer-Verlag, Berlin, 1955) pp. 325-382.

23. R. M. Bozorth, Ferromagnetism, (D. Van Nostrand Co., Inc., Princeton, New Jersey, 1951).

24. J. A. Hofman, et al., J. Phys. Chem. Solids, 1, 45(1956).

25. A. H. Wilson, in Thermodynamics and Statistical Mechanics, (Cambridge University Press Cambridge, 1957) Chap. 10.

26. C. Kittel, Quantum Theory of Solids, (John Wiley and Sons, Inc., New York, 1963).

27. L. Patrick, Phys. Rev., 93, 384(1954).

28. J. M. Léger et al., Sol. Stat. Comm. 4, 503(1966).

29. H. S. Carslaw and J. C. Jaeger, Conduction of Heat in Solids, (Oxford University Press, London, 1959).

30. See, for example, C. C. Bradley, High Pressure Methods in Solid State Reasearch, (Butterworths, London, 1969).

31. F. R. Boyd, in Modern Very High Pressure Techniques, edited by R. H. Wentorf, (Butterworths, London, 1962).

32. Temperature, Its Measurement and Control in Science and Industry, vol. I, (Reinhold, New York, 1941).

33. F. P. Bundy, Effect of Pressure on EMF of Thermocouples, in Progress in Very High Pressure Research, edited by F. P. Bundy, W. R. Hibbard, Jr., H. M. Strong, (John Wiley and Sons, Inc., New York 1961).

34. Temperature, Its Measurement and Control in Science and Industry, vol. II, edited by H. C. Wolfe, (Reinhold, New York, 1955).

35. H. Drickamer, A. Balchan, Rev. Sci. Inst. 32, 308(1961).

36. K. Kelley, J. Chem. Phys. 11, 16(1943).

37. F. Nix and D. NcNair, Phys. Rev. 60, 597(1941).

38. F. Seitz, The Modern Theory of Solids, (McGraw-Hill Book Co., New York, 1940).

PART 2. FERMI MOMENTUM OF Yb AT HIGH PRESSURE

I. INTRODUCTION

At atmospheric pressure, Europium and Ytterbium differ from the other Lanthanide metals in that they do not have 5d electrons in the ground state of the metal. This difference in electronic structure leads to marked differences in physical properties. It was postulated by Hall, Barnett, and Merrill that Yb reverts to a normal Lanthanide at the 40 kbar phase transition.[5,6] The pressures and temperatures at which Eu may similarly revert are beyond the capabilities of the experimental arrangement in use in this laboratory. Ytterbium, however, can be easily studied, and the discussion is restricted to this metal.

Magnetic susceptibility measurments by Lock indicated that Yb metal has a filled 4f shell and, therefore, can have only two conduction electrons per atom[3]. A typical Lanthanide has three donduction electrons per atom. Ytterbium metal has fair electrical conductivity and the predominant carriers have been shown to be holes[2]. Under ordinary conditions it has a non-typical Lanthanide crystal structure-fcc, unusually low density and high compressibility[1]. In most of its chemical compounds, however, Yb does exhibit typical Lanthanide behavior. It normally forms compounds of Yb^{3+}. It can, however, also form compounds of Yb^{2+}. This latter is not typical behavior for a Lanthanide.

As Yb is subjected to increasingly high pressures, a number of changes occur in its properties[4]. Initially it exhibits an electrical resistivity of about 30 μohm-cm, and a positive temperature coefficient of resistivity. The resistivity rapidly increases with increasing

pressure. Above a pressure of 20 kbar it exhibits a negative temperature coefficient of resistivity. This behavior of the resistivity is not completely understood. There are at least two possible explanations. These are the unlapping of the conduction bands with pressure, and an increase in the resonance scattering of the conduction electrons with pressure. The former explanation is generally accepted. If that explanation is valid, the data indicate that fcc Yb becomes a semiconductor under pressure. The apparent band gap increases with pressure up to about 40 kbar. At that pressure there is a phase transition from fcc to bcc. The bcc phase is metallic in nature. At the phase transition there is about a 3% decrease in volume. Ytterbium then exhibits a typical Lanthanide metallic radius. Basing their conclusions on a hard sphere model, Hall, Barnett, and Merrill postulated that Ytterbium does indeed become a normal Lanthanide after the transition.[5,6] They, therefore, proposed that in the high pressure phase Yb has three conduction electrons per atom. No direct test of this hypothesis had been made up to the work presented herein.

II. POSITRON ANNIHILATION

An energetic positron which enters a metal is thermalized to room temperature in about 3×10^{-12} sec[7]. Since the lifetime of a positron in a Lanthanide metal is greater than 2×10^{-10} sec[8], it is probable that a positron is thermalized before it annihilates. The ordinarily observed event is the two gamma annihilation.

In simple metals, after the positron is thermalized it has a small probability of penetrating to the atomic cores because of simple Coulomb repulsion. If the cores are small the positron will annihilate predominantly with conduction electrons. Annihilations with core electrons are more probable in transition metals, and there is usually a considerable background associated with these annihilations. The momentum distribution of the conduction electrons outside the core is adequately described for the purposes of this experiment by a simple free electron model. That is, the density of states of conduction electrons in momentum space is a constant up to the Fermi momentum, p_F, and zero above it. The Fermi momentum is given by the expression

$$p_F = \hbar(3\pi^2 N/V)^{1/3} ,$$

where N/V is the density of conduction electrons in real space.

The angular correlation distribution due to the conduction electrons can be calculated if it is assumed that the positron equally samples and does not perturb the conduction electrons. If, as is the normal case, the apparatus can resolve momentum, $\bar{p}$, in one direction only, taken to be the z direction, then the measured angular correlation intensity curve, $I(p_z)$, will be

$$I(p_z) = C(p_F^2 - p_z^2) \text{ , } p_z < p_F \text{ ,}$$

$$= 0 \text{ , } p_z > p_F \text{ ,}$$

where C is a constant determined by the conditions of the experiment.

$$p_z = mc\Theta, \ \Theta \text{ small,}$$

where m is the mass of an electron (or positron), c is the speed of light, and Θ is the angle between the emitted gamma rays measured in the z direction.

The expected curve is an inverted parabola which goes to zero at the Fermi momentum. A parabola of the expected width has been found for many metals.[9-11] The parabola is invariably superimposed on a broad background. This background is presumably due to annihilations with core electrons. If the number of conduction electrons changes from two to three, as may be expected at the phase transition in Yb, the width of the measured curve will change by a factor of $(3/2)^{1/3}$. This is a change of over 14%.

III. EXPERIMENTAL

The positron source consisted of about 1.5 m Ci of "carrier free" $Na^{22}Cl$. This material was placed between two discs of Mylar about 6.5 mm in diameter and 0.006 mm thick. These Mylar discs were cemented together to form a sealed source. This source assembly was placed between two discs of Yb metal 7.9 mm in diameter and 0.18 mm thick. The high pressures were applied to this assembly using a set of opposed Bridgman anvils. The anvils had face diameters of 12.7 mm. Two pyrophyllite retaining rings each 12.7 mm in diameter and 0.254 mm high were used to complete the high pressure cell. Electrical leads were admitted between these rings. This made it possible to monitor the electrical resistivity of the sample so that it was known whether or not the transition had occurred. This also served as a secondary check on the pressure.

The angular correlation apparatus was constructed with horizontal slits to take advantage of the small vertical dimension of the sample. The slits were each 0.51 mm high and 1.02 m from the source. The detectors were 5.1 cm NaI(Tl) scintillators.

It is known from previous experience with a source prepared in the same way as the one used here at less than one half of one percent of the non-random coincidences came from within the Mylar and NaCl source material. Also it has been calculated that less than one percent of the coincidences which were detected came from annihilations within the Bridgman anvils. This latter fact results from the large absorption of the gamma rays by the tungsten carbide anvil material. No corrections were made for these two sources of non-random coincidences. The data were corrected for random coincidences and decay of

the source. A correction was also made for a small angular dependence of counting rate. This angular dependence results from the fact that some of the gamma rays were blocked by the anvil faces at large angles. None of these corrections exceeded 5%.

IV. RESULTS

Angular correaltion curves were taken at nine different pressures from one atmosphere to 80 kbar. It was found that the points taken at angles beyond the central parabolic region could be fit very well by a sum of two Gaussian curves. Gaussian curves were chosen for purely empirical reasons. Points taken beyond about 11 mrad from the center of the distribution were fit with one Gaussian. All the points were corrected for this minor contribution. The corrected points taken between 6 and 11 mrad from the center were fit with a second Gaussian. All of the points were corrected for this contribution. This was a large correction. The background represented by these two Gaussians is thought to be the result of annihilations with electrons in core states. This background changed very little with pressure. The low angle points, after correcting for this background, could be fit very well with an inverted parabola. The width of this parabola was not strongly dependent on exactly how the background was corrected for.

A typical angular correlation curve is shown in Fig. 1. The dashed curves are the two Gaussians. The lower solid curve is the inverted parabola. The solid curve through the points is the sum of these three curves.

The widths of the fitted curves are shown in Fig. 2 as a function of pressure. Also shown is the predicted behavior of the width. This prediction was based on the free electron theory. Calculated values are shown on the assumption of both two and three conduction electrons per atom. An initial density of 6.98 g/cm^3 for Yb metal was used.[1] The pressure volume data which were used in the calculation are those of Stevens.[12] His data extend only to just past the phase transition

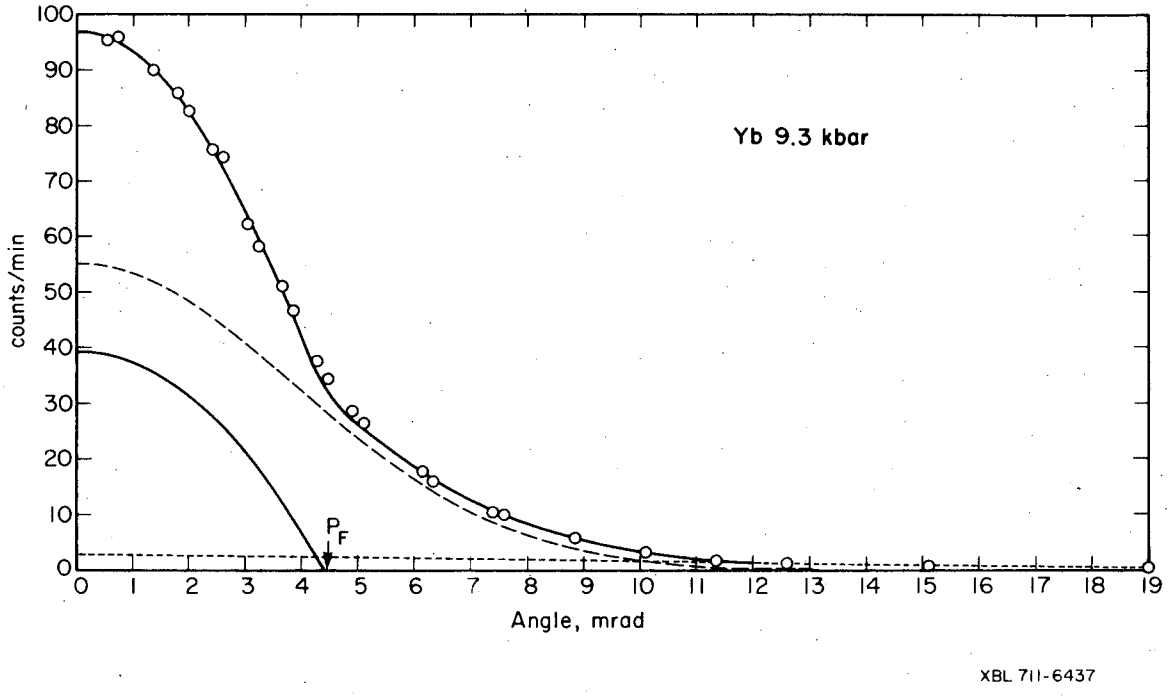

Fig. 1. Angular Correlation curve for Yb at 9.7 kbar

at 40 kbar. Two different approximations were used to estimate the density of Yb up to 85 kbar. The upper dashed curve assumes that Yb at 85 kbar has the same density as a normal Lanthanide would have at 45 kbar. This probably overestimates the compressibility because the density of bcc Yb at 40 kbar is still less than that of a normal Lanthanide at 1 atm. The lower dashed curve assumes that the compressibility of Yb from 40 to 85 kbar is the same as the compressibility of a normal Lanthanide from 0 to 45 kbar. It is felt that this is a more reasonable estimate of the compressibility. Fortunately the Fermi momentum is sufficiently weakly dependent on the volume that it is unambiguous as to whether two or three conduction electrons are present.

V. DISCUSSION

It is evident from Fig. 2 that this experiment indicates that there are only two conduction electrons per atom in both the fcc and bcc phases of Yb metal. This seems reasonable in retrospect.

The first published postulation of three conduction electrons per atom in the bcc phase appears to have been advanced by Hall, Barnett, and Merrill, who determined the high pressure crystal structure of Yb metal.[5,6] They considered only nearest neighbor distances in comparison of the two crystal structures. They also, evidently, assumed that these distances were determined by the interaction of hard atomic cores. It became necessary for them to propose an unusual mechanism in order to explain the transition from a close packed to a non-close packed structure with increasing pressure. To explain the observed decrease in nearest neighbor distance they proposed that the atomic core had changed. The only rational change appeared to be from a (Xe) $4f^{14}$, 2+ core to a (Xe)$4f^{13}$, 3+ core. The expelled electron would go into either a 5d or 6p conduction band since the 6s band is already full.

This change in the core is not unreasonable. After all, configurations of the type (Xe)$4f^n5d^06s^2$ are the stable configurations of the free atoms for all of the Lanthanides except La, Ce, Gd, Lu, and possibly Tb.[13] Yet, in the metals the stable configurations are of a type (Xe)$4f^{n-1}5d^16s^2$, except for Eu and Yb which tend to maintain a half filled and filled f shell respectively. In most of the Lanthanides, then, the solid state interactions are able to shift the former atomic states enough so that a core with one less f electron than exists in the free atom is stable. The 5d and 6s electrons in

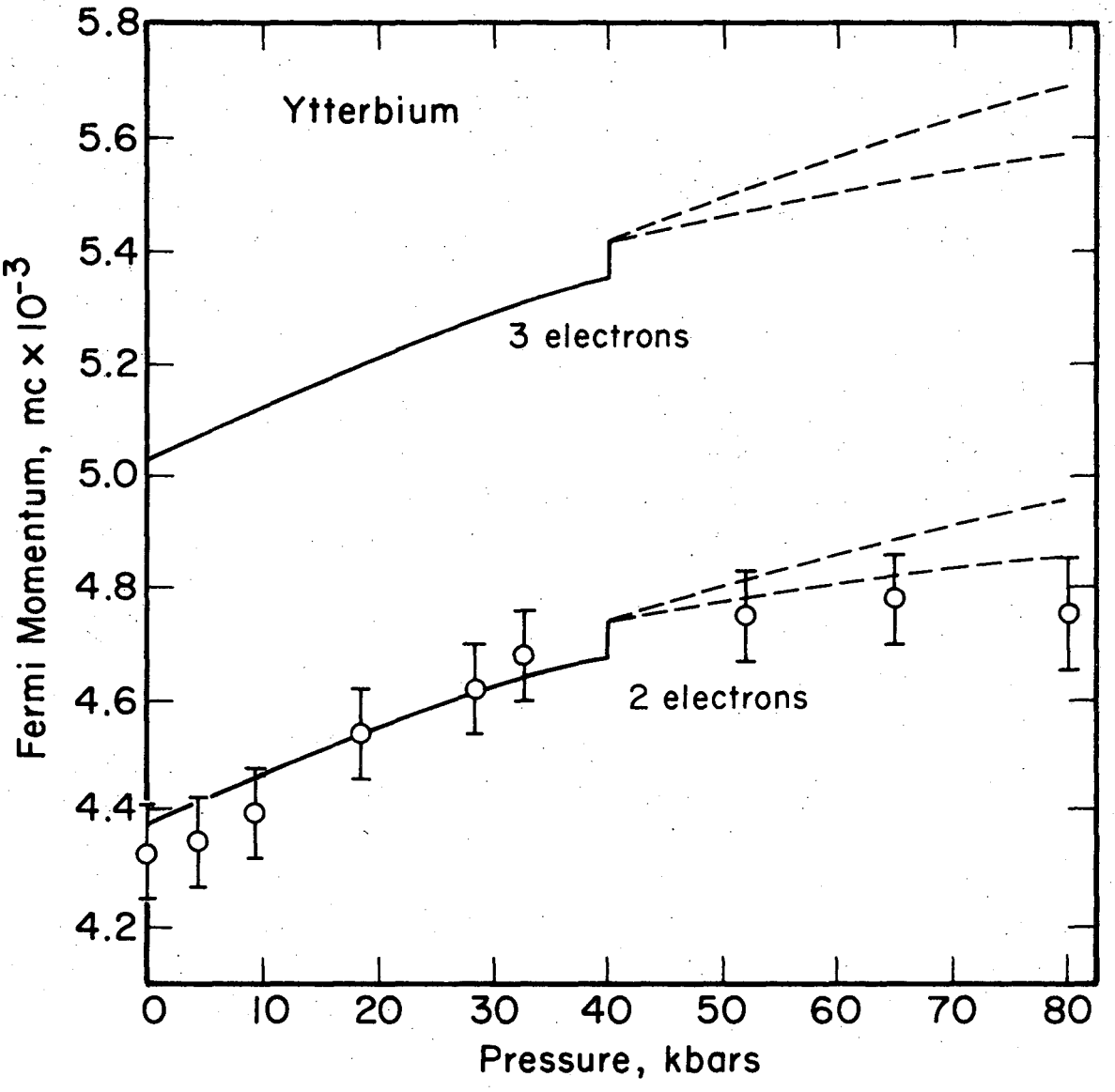

Fig. 2. Effect of pressure on the Fermi momentum of ytterbium.

the metal are, of course, actually in conduction bands which have nodal properties at the core like d and s electorns.

There are some differences, to be sure, between Yb and a typical Lanthanide such as its neighbor, Tm. Recently Brewer[14] has collated data on the atomic configurations of many elements. The energies of come configurations have been estimated. His work indicates that for an isolated Yb atom the $(Xe)4f^{14}6s^2$ configuration lies 3.1 ± .2 ev below the lowest $(Xe)4f^{13}5d^16s^2$ configuration and 3.9 ± .2 ev below the lowest $(Xe)4f^{13}6s^26p^1$ configuration. In atomic Tm, on the other hand, the lowest $(Xe)4f^{13}6s^2$ configuration is only 1.6265 ev below the lowest $(Xe)4f^{12}5d^16s^2$ configuration and 2.7856 ev below the lowest $(Xe)4f^{12}6s^26p^1$ configuration.[15,16] The energy differences are 1.5 ev greater in Yb than in Tm. This is a large enough difference to suggest the possibility that a 3+ core amy not be obtained in Yb metal even though it is obtained in Tm metal.

Hall, Barnett, and Merrill unfortunately overlooked several other points. One is that although the interatomic distance is over 6a.u. after the fcc-bcc phase transition, the diameter of a $(Xe)4f^{14}$, 2+ core probably does not exceed 5a.u. The maximum in the 4f electron distribution in such a core has a diameter of less than 2a.u., and the maximums for the 5s and 5p electrons have diameters of about 3a.u. In its divalent compounds Yb is estimated to have a diameter of about 4a.u.[17] Such a core can still be accomodated in the new crystal structure.

In addition to these facts, the bcc structure may actually be considered to be a more closely packed structure than fcc if a hard sphere model is not used. The fcc structure has 12 nearest neighbors

and 6 next nearest neighbors 41% further away. The bcc structure has 8 nearest neighbors and 6 next nearest neighbors only 15% further away. After the phase transition the next nearest neighbors are only 12% further away than the nearest neighbors were in the fcc structure. If next nearest neighbor interactions are important, it no longer becomes necessary to invoke any extraordinary phenomenon in order to explain the transition from a so called close packed structure to a non-close packed structure under the influence of pressure.

This argument is further supported by the remarkable similarities between Yb and Sr metals. These similarities are discussed by Jayaraman.[18] Both metals are face centered cubic at one atmosphere, and they have similar electrical resistivities. The resistivities of both increase an order of magnitude between 1 atm. and 35 kbar. Both appear to be semiconductors above 10 kbar. Strontium assumes a bcc structure at 35 kbar and Yb at 40 kbar. Both are good metals after the transition. With such striking parallels it seems natural to attempt to explain the behavior of both metals by the same mechanism. Clearly any mechanism which explains the Yb transition on the basis of the promotion of a 4f electron to a conduction band is entirely inappropriate for Sr. Strontium has no electrons which could conceivably be promoted to a conduction band.

The explanation of the resistance behavior evidently appears to lie in the premise that the first and second bands are unlapping with pressure. This leads to the semiconducting behavior. The first two bands are strongly overlapped after the phase transition, resulting in metallic conduction. The phase transition may take place just

because the new phase allows for a lowering of the average energy of the conduction electrons because of the overlap of the first two conduction bands.

ACKNOWLEDGEMENTS

I am most grateful to Professor George Jura for guiding this work with wisdom, insight, and patience, and for providing sympathy during my frequent periods of frustration. He has made my entire stay at Berkeley an invaluable experience.

My wife was a major source of inspiration and encouragement. Her patience and understanding have been most wonderful and are deeply appreciated.

I also wish to thank Dr. John Przybylinski for his many helpful suggestions, Mr. Tang-hua Chen for his generous help and stimulating discussions, Mr. Duane Newhart and Mr. Donald McClure for expert and ingenious technical assistance.

My gratitudes also go to many other individuals both at the Chemistry Department here and at the Lawrence Berkeley Laboratory who were helpful.

This work was performed under the auspices of the United States Atomic Energy Commission.

APPENDIX I

CONSTANT CURRENT PULSE GENERATOR

Most constant current power supplies are based on the principle of amplifying the difference between a signal proportional to the current passing through the load and a signal provided by a reference voltage source. The amplified difference, or error, signal is used to drive a transistor which has the effect of changing its transconductance. The transconductance is changed in a way that will tend to decrease the error signal. This feedback eventually regulates the current such that it fluctuates around a constant value, the amount of fluctuation depending on the stability of the reference voltage source, the sensitivity of the error amplifier and a number of other less significant factors. The speed of response to changing loads depends on both the error amplifier and the regulating transistor, or transistors. The most obvious way to design a current pulse generator is to provide the error amplifier with a reference voltage pulse of the desired duration and magnitude. Obviously how constant and sharp the current pulse is depends heavily on these same qualities of the reference voltage pulse. Fortunately such a voltage pulse can be easily generated by a device built from a commercially available integrated circuit operational amplifier.

The National Semiconductors operational amplifier LM201 can be used as a comparator which compares an external signal with a reference voltage; as soon as the external signal equals or exceeds the reference voltage the output produces a signal that can be clamped to any voltage less than 15 volts. A zener diode is used to provide the reference voltage. A monostable-multivibrator Fairchild 9601 upon

the application of a trigger produces a variable duration pulse which is larger than the zener reference voltage. When this pulse is applied to the external signal input of the LM201 comparator a pulse of the same duration appears at its output, clamped by another zener diode. The 1N939A, which is a very stable and fast reference diode, when used to clamp the output results in a 9.45 volt pulse that has a reasonably fast rise time of about 20 μsec. and an extremely "flat" top. Efforts to produce faster rise times by using other clamping diodes created such undesirable side effects as overshoot, ringing, droop, high frequency oscillations or a combination of several of these effects. The use of the 1N939A was therefore a necessary compromise. This very high quality voltage pulse is then sent into a voltage divider which selects the value of the current pulse to be produced. The output of the voltage divider is now used as the reference voltage signal for the error amplifier, a LM301A integrated circuit operational amplifier. The output of the LM301A is fed into the base of a Darlington pair formed by a 2N3019 and two 2N3716 in parallel. The collectors of this Darlington pair are connected to any voltage source capable of delivering 15 volts at 10 amps. The emitters of the two 2N3716 are connected to the load. The same current that flows through the load flows through a shunt with a large heat capacity which provides the feedback signal for the other input of the LM301A. Careful layout of the components and wires is necessary to avoid accidental 60 Hz noise pick up and oscillations.

The generator is capable of producing 10 amp pulses with a 15 volt compliance for practically any duration longer than the rise time. The final rise time is approximately 25 μsec. and its exact shape is

dependent on the reactance presented by the load and the power source used. The constancy of the pulse is impossible to measure using presently commercially available test instruments and has been conservatively estimated to be better than .05%. (The Tektronix Type W plug-in amplifier, which has a sensitivity of 1mv/cm and has a comparator which theoretically enables one to measure pulses with a resolution of one part in 100,000 cannot be used to measure the constancy of the pulses produced because in practice, when using the highest sensitivity a pulse that is more than a few hundred millivolts produces a distortion which makes the pulse appear not very constant. The drift of this amplifier also renders it useless for measuring the absolute magnitude of the pulse.)

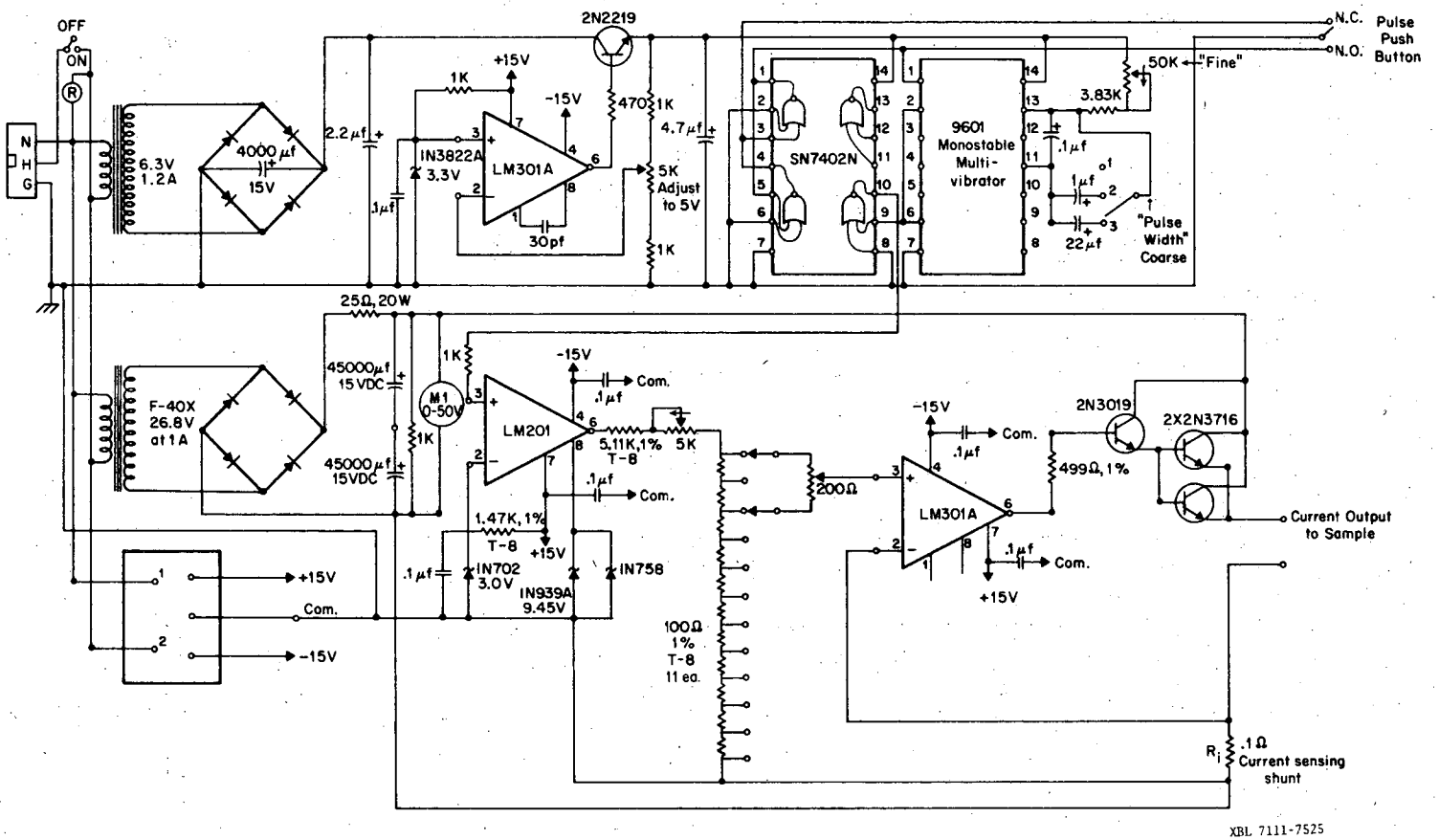

Fig. AI.1. Circuit diagram of the constant current pulse generator.

APPENDIX II

HEAT CAPACITY DATA
(C_p in arbitrary units)

Temperature °K	Pressure kbar 25	35	45	75
110.4	44.7	44.2	43.3	
120.4	48.6	47.8	48.0	46.7
130.4	52.6	52.4	51.9	52.3
140.0	55.6	55.3	55.9	55.2
150.4	58.8	58.9	58.9	59.9
160.4	61.9	61.6	60.9	61.1
170.4	64.2	63.7	63.4	63.8
180.4	66.0	66.5	65.8	66.5
190.4	68.5	68.1	68.5	67.7
200.4	71.4	69.9	70.1	69.5
210.4	72.1	71.9	71.2	73.0
220.4	73.3	73.0	73.4	73.3
230.3	75.0	74.5	74.0	74.2
240.4	76.4	76.1	76.3	
250.4	77.8		77.3	79.2
260.4	79.0	78.3		78.7
270.4	79.8	79.9	80.3	79.7
280.0	79.5			

PART 2. REFERENCES

1. Rare Metals Handbook, 2nd edition, (Reinhold Publishing Corp., New York, 1961), pp 402-7.
2. G. S. Anderson, S. Legvold, F. H. Spedding, Phys. Rev. 111, 1257 (1958).
3. J. M. Lock, Proc. Phys. Soc. 70B, 476(1957).
4. P. C. Souers, G. Jura, Science 140, 481(1963).
5. H. T. Hall, J. D. Barnett, L. Merrill, Science 139, 111(1963).
6. H. T. Hall, L. Merrill, Inorg. Chem. 2, 618(1963).
7. G. E. Lee-Whiting, Phys. Rev. 97, 1557(1955).
8. J. L. Roda, M. G. Stewart, Phys. Rev. 131, 255(1963).
9. G. Lang, S. DeBenedetti, Phys. Rev. 108, 914(1957).
10. A. T. Stewart, Can. J. Phys. 35, 168(1957).
11. D. R. Gustafson, A. R. Mackintosh, J. Phys. Chem. Solids 25, 389 (1964).
12. D. R. Stevens, J. Phys. Chem. Solids 25, 423(1964).
13. W. F. Meggers, Rev. Mod. Phys. 14, 96(1942).
14. L. Brewer, Private Communication.
15. P. Camus, J. Blaise, Compt. Rend. 261, 4359(1965).
16. P. Camus, J. de Phys. 27, 717(1966).
17. T. Moeller, The Chemistry of the Lanthanides, (Reinhold Publishing Corp., New York, 1963), p 20.
18. A. Jayaraman, Phys. Rev. 135, A1056(1964).

TECHNICAL INFORMATION DIVISION
LAWRENCE BERKELEY LABORATORY
UNIVERSITY OF CALIFORNIA
BERKELEY, CALIFORNIA 94720